

1  
2 **Distributed summer air temperatures across mountain glaciers in the**  
3 **south-east Tibetan Plateau: temperature sensitivity and comparison**  
4 **with existing glacier datasets**  
5

6 Thomas E. Shaw<sup>1</sup>, Wei Yang<sup>2,3</sup>, Álvaro Ayala<sup>4</sup>, Claudio Bravo<sup>5</sup>, Chuanxi Zhao<sup>2</sup>, Francesca  
7 Pellicciotti<sup>1,6</sup>  
8

9 <sup>1</sup> Federal Institute for Forest, Snow and Landscape Research (WSL), Birmensdorf, Switzerland

10 <sup>2</sup> Key Laboratory of Tibetan Environment Changes and Land Surface Processes, Institute of  
11 Tibetan Plateau Research, Chinese Academy of Sciences (CAS), Beijing, China

12 <sup>3</sup> CAS Center for Excellence in Tibetan Plateau Earth Sciences, Beijing 100101, China

13 <sup>4</sup> Centre for Advanced Studies in Arid Zones (CEAZA), La Serena, Chile

14 <sup>5</sup> School of Geography, University of Leeds, Leeds, UK

15 <sup>6</sup> Department of Geography, Northumbria University, Newcastle, UK  
16

17 T E Shaw: ORCID: 0000-0001-7640-6152

18 A Ayala: ORCID: 0000-0003-2241-0521

19 C Bravo: ORCID: 0000-0003-4822-4786

20 *Corresponding author: Thomas E. Shaw ([thomas.shaw@wsl.ch](mailto:thomas.shaw@wsl.ch))*  
21

22 **Keywords:** Air Temperature, Glaciers, Tibetan Plateau, temperature sensitivity  
23

24 **Abstract**

25 Near-surface air temperature ( $T_a$ ) is highly important for modelling glacier ablation, though its  
26 spatio-temporal variability over melting glaciers still remains largely unknown. We present a new  
27 dataset of distributed  $T_a$  for three glaciers of different size in the south-east Tibetan Plateau during  
28 two monsoon-dominated summer seasons. We compare on-glacier  $T_a$  to ambient  $T_a$  extrapolated  
29 from several, local, off-glacier stations. We parameterise the along-flowline sensitivity of  $T_a$  on  
30 these glaciers to changes in off-glacier temperatures (referred to as temperature sensitivity) and  
31 present the results in the context of available distributed on-glacier datasets around the world.  
32 Temperature sensitivity decreases rapidly up to 2000-3000 m along the down-glacier flowline  
33 distance. Beyond this distance, both the  $T_a$  on the Tibetan glaciers and global glacier datasets  
34 show little additional cooling relative to the off-glacier temperature. In general,  $T_a$  on small  
35 glaciers (with flowline distances < 1000 m) is highly sensitive to temperature changes outside the  
36 glacier boundary layer. The climatology of a given region can influence the general magnitude of  
37 this temperature sensitivity, though no strong relationships are found between along-flowline  
38 temperature sensitivity and mean summer temperatures or precipitation. The terminus of some  
39 glaciers is affected by other warm air processes that increase temperature sensitivity (such as  
40 divergent boundary layer flow, warm up-valley winds or debris/valley heating effects) which are  
41 evident only beyond ~70% of the total glacier flowline distance. Our results therefore suggest a  
42 strong role of local effects in modulating temperature sensitivity close to the glacier terminus,  
43 although further work is still required to explain the variability of these effects for different  
44 glaciers.

45  
46 **1. Introduction**

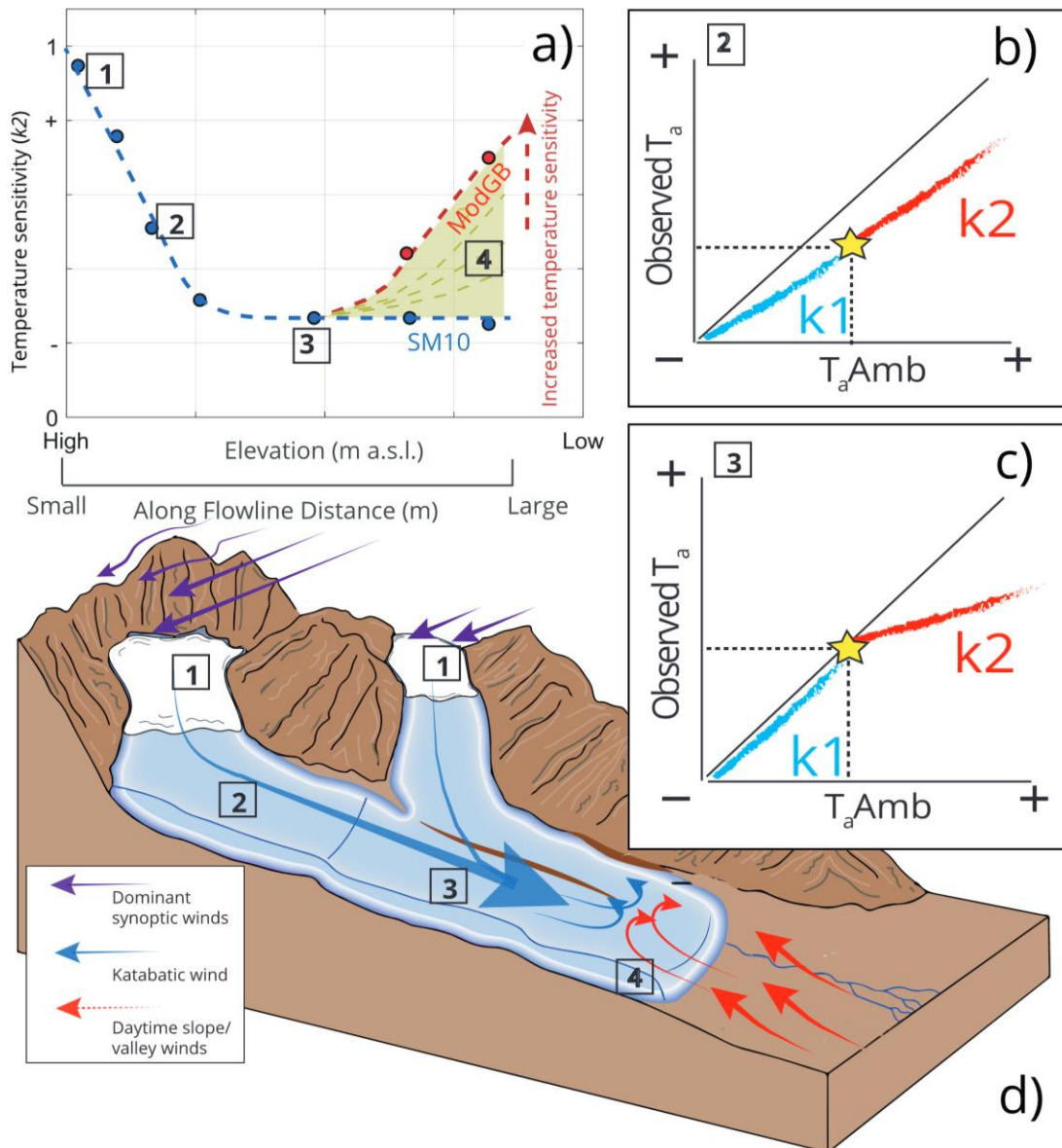
47 Near-surface air temperature ( $T_a$ ) is one of the dominant controls on glacier energy and mass  
48 balance during the ablation season (Petersen et al., 2013; Gabbi et al., 2014; Sauter and Galos,  
49 2016; Maurer et al., 2019; Wang et al., 2019), though modelling its spatio-temporal behaviour  
50 above melting ice surfaces remains a challenge. The absence of distributed information regarding  
51  $T_a$  has favoured the use of simple, space-time invariant relationships of  $T_a$  with elevation, typically  
52 that of the free-air environmental lapse rate (*ELR*). A free-air ELR cannot be reliably used to  
53 estimate near-surface air temperatures above melting glaciers, where steep gradients are found  
54 within 10 m of the surface under warm ‘ambient’ (off-glacier) conditions (van den Broeke, 1997;  
55 Greuell and Böhm, 1998; Oerlemans, 2001; Oerlemans and Grisogono, 2002; Ayala et al.,  
56 2015). As a result, any extrapolation of  $T_a$  observations from an off-glacier location, particularly  
57 those at lower elevations, are likely to lead to an overestimation of snow and ice ablation in energy  
58 balance and enhanced temperature index melt simulations (e.g. Petersen and Pellicciotti, 2011;  
59 Pellicciotti et al., 2014; Shaw et al., 2017). While models applying the degree day approach can  
60 make use of off-glacier temperatures as forcing because they are heavily reliant on calibration,  
61 for energy balance models and models of intermediate complexity (Pellicciotti et al., 2005;  
62 Ragetti et al., 2016) it is key to resolve the air temperature distribution over glaciers, especially  
63 for turbulent flux calculations and typical parameterizations of incoming longwave radiation.

64  
65 This problem has been long understood (Greuell et al., 1997; Greuell and Böhm, 1998), but only  
66 within the last decade have studies approached it in more detail (Petersen et al., 2013; Ayala et  
67 al., 2015; Carturan et al., 2015; Shaw et al., 2017; Bravo et al., 2019a; Troxler et al., 2020). Until  
68 recently, modelling studies have relied upon simple lapse rates (including the *ELR*) and/or single  
69 bias offset values to account for the ‘cooling effect’ of the near-surface air on-glacier (Arnold et  
70 al., 2006; Nolin et al., 2010; Ragetti et al., 2016). The variations of  $T_a$  along the glacier flowline  
71 (defined following Shea and Moore (2010) as the horizontal distance from an upslope summit or  
72 ridge), however, are much more complex (Ayala et al., 2015; Shaw et al., 2017), though a lack of  
73 available data usually restricts one’s ability to appropriately model this variable.

74 To date, two main, simplified model approaches have been developed and tested to represent air  
75 temperature over glaciers (Figure 1a). The first is the statistical model by Shea and Moore (2010)  
76 developed to reconstruct  $T_a$  across glaciers of varying size in western Canada from ambient  
77 temperature records. This approach considered the ratios of observed on-glacier temperature and  
78 estimated ambient temperature for the elevation of a given point on a glacier (hereafter ‘ $T_{aAmb}$ ’).  
79 The authors calculated two ratios from a piecewise regression above and below a critical threshold  
80 temperature for the onset of the glacier katabatic boundary layer (*KBL* - see section 4.3). The  
81 parameterisations that operate as a function of the along-flowline distance have since been tested  
82 by Carturan et al. (2015) and Shaw et al. (2017) on smaller glaciers in different parts of the Italian  
83 Alps. Carturan et al. (2015) found that the original published parameterisations were sufficient to  
84 explain  $T_a$  on small, fragmenting glaciers up to flowline distances of ~2000m. However,  
85 investigation by Shaw et al. (2017) on a small alpine glacier found a pattern of along-flowline  $T_a$   
86 that was better described by an alternative, thermodynamic model approach. This second,  
87 physically-oriented approach was developed by Ayala et al. (2015) to account for a relative  
88 ‘warming effect’ evident on the termini of some mountain glaciers when compared to upper  
89 elevations. The modified model (termed ‘ModGB’ in the literature) accounts for the down-glacier  
90 cooling of  $T_a$  at increasing flowline distances due to sensible heat exchange and adiabatic heating  
91 (Greuell and Böhm, 1998). It adds a warming factor based upon on-glacier observations in the  
92 lower sections of the glacier (e.g. at the greatest flowline distances) to account for additional  
93 processes of adiabatic warming (Ayala et al., 2015) (Figure 1a). The ModGB approach has been  
94 successively applied at other glacier sites around the world (Shaw et al., 2017; Troxler et al.,  
95 2020), though the question of its transferability remains open (Troxler et al., 2020).

96 In this way, the ModGB method operates on the physical principles of the glacier boundary layer  
97 (Greuell and Böhm, 1998) though it corrects for relative warming on the lower portion of glacier  
98 (Ayala et al., 2015). To establish the magnitude of this warming, however, along-flowline data in  
99 the lower portion of the glacier are essential. Because the available distribution of on-glacier  
100 observations is often limited and rarely extends for the entire length of the glacier flowline, this  
101 additional correction for warming associated with the unknown parameters of ModGB can lead

102 to high variability in  $T_a$  estimates on the lower glacier ablation zone (Troxler et al., 2020) (Figure  
 103 1a). In contrast to this, the statistical method of Shea and Moore (2010) provides a more  
 104 simplified estimation that has fewer assumptions and parameters, though it does not explicitly  
 105 account for physical processes thought to be the cause of ‘relative warming’ on the glacier  
 106 terminus. It also provides a parameter that more explicitly represents the glacier ‘temperature  
 107 sensitivity’ of the on-glacier  $T_a$  (defined here as the ratio of changes in observed  $T_a$  on-glacier to  
 108 changes in  $T_{aAmb}$  - Figure 1b and 1c). Despite its more conceptual nature, because of its ease of  
 109 applicability, typical of a more simplistic statistical approach, we adopt the Shea and Moore  
 110 (2010) method to further investigate along-flowline  $T_a$  in this study.  
 111



112  
 113 *Figure 1: A schematic diagram to describe the temperature sensitivity of on-glacier air temperature ( $T_a$ )*  
 114 *to the extrapolated ambient temperature ( $T_{aAmb}$ ) at given elevations/flowline distances on a mountain*  
 115 *glacier. Points 1-4 indicate locations of interest that are linked between panels. Panel (a) indicates*  
 116 *the along-flowline ‘ $k_2$ ’ temperature sensitivities to  $T_{aAmb}$ , considering the differences represented by the*  
 117 *models of SM10 and ModGB for glacier termini (see text). Panels (b) and (c) represent the differences of*  
 118  *$k_1$  (blue) and  $k_2$  (red) sensitivities observed in the data at different theoretical locations on the glacier,*  
 119 *the latter of which shows the theoretical parameterisation presented by Shea and Moore (2010). The yellow*  
 120 *stars indicate the calculated threshold for katabatic onset ( $T^*$  in the text). Panel (d) represents an idealised*  
 121 *case of katabatic and valley/synoptic wind interactions that potentially dictate the along-flowline structure*  
 122 *of on-glacier temperature sensitivity and thus  $T_a$  estimation.*

123  
124  
125  
126  
127  
128  
129  
130  
131  
132  
133  
134  
135  
136  
137  
138

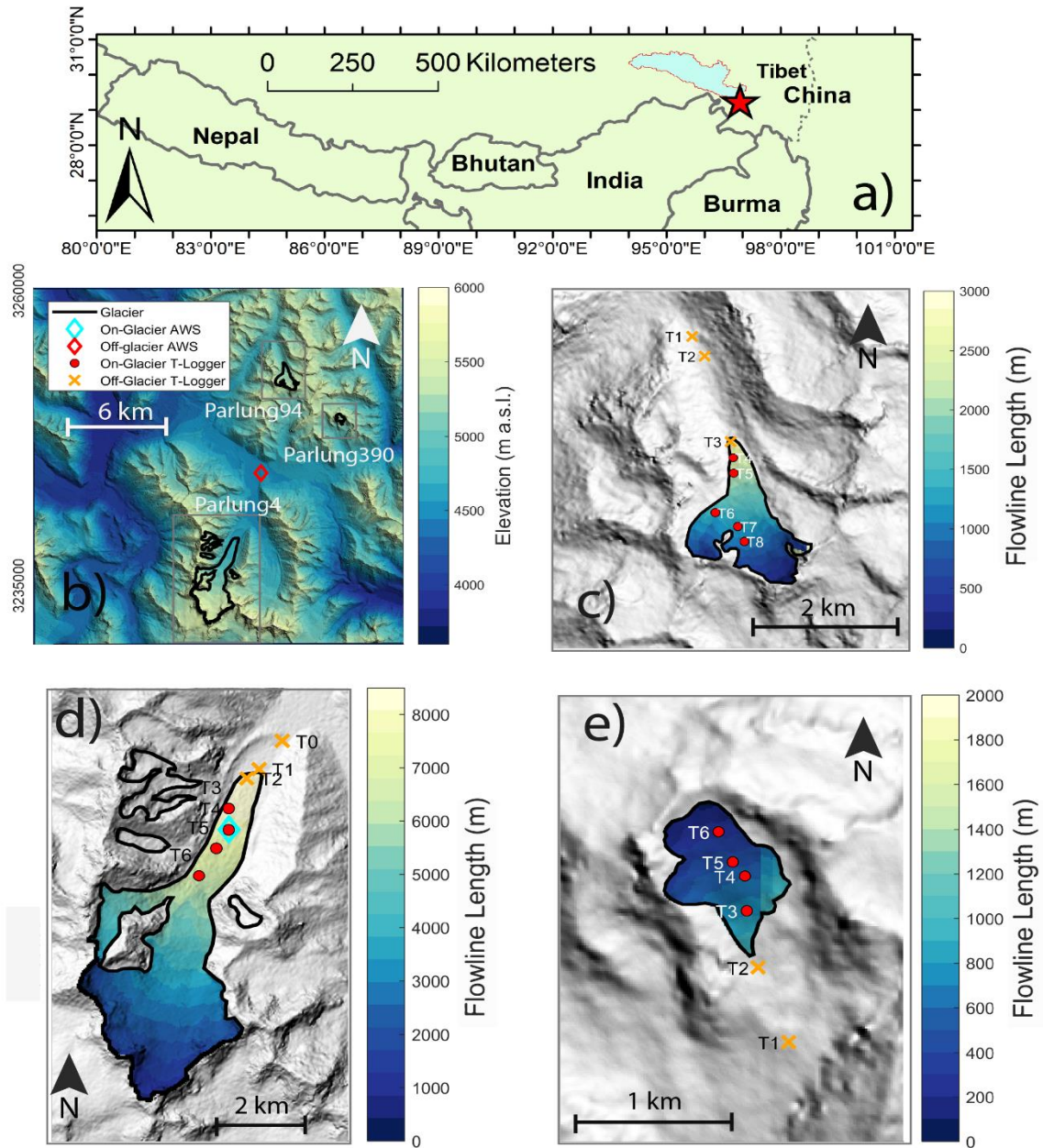
To date, few studies have investigated the variability of distributed, on-glacier  $T_a$  at different sites around the world. As such, the transferability of temperature estimation models and/or model parameters remain mostly unknown, and analysis of individual glacier sites, while beneficial to process understanding, may not advance the science on how to treat the on-glacier  $T_a$  in models. In this study, we use new datasets of on-glacier temperature observations on three glaciers of varying size in the south-east Tibetan Plateau. We analyse the main controls on along-flowline  $T_a$  and its temperature sensitivity and present these new findings in the context of 11 other on-glacier observations around the world.

Specifically we aim to i) understand the variability of  $T_a$  with the along-flowline distances at three glaciers in the south-east Tibetan Plateau, ii) identify and quantify the temperature sensitivity of on-glacier  $T_a$  for different meteorological conditions and glacier sizes and iii) parameterise the along-flowline  $T_a$  using the Shea and Moore (2010) method for the Tibetan glaciers and discuss it in the context of globally-derived, published datasets of on-glacier air temperatures.

139  
140  
141  
142  
143  
144  
145  
146  
147  
148  
149  
150  
151  
152  
153  
154  
155  
156  
157  
158  
159  
160

**2. Study Site**

The study glaciers are located in the upper Parlung-Zangbo River catchment in the southeast Tibet Plateau (29.24°N, 96.93°E - Figure 2), a region characterised by a summer monsoon climate that typically intrudes via the Brahmaputra Valley (Yang et al., 2011). We present data for three maritime-type valley glaciers in the Parlung-Zangbo catchment: Parlung Glacier Number 4 (hereafter ‘Parlung4’), Parlung Glacier Number 94 (‘Parlung94’) and Parlung Glacier Number 390 (‘Parlung390’). Parlung4 (Figure 2d) is ~10.8 km<sup>2</sup>, north-northeast facing and has an elevation range of 4659-5939 m a.s.l. (Ding et al., 2017). Glaciers Parlung94 (Figure 2c) and Parlung390 (Figure 2e) are smaller valley glaciers (2.51 and 0.37 km<sup>2</sup>, respectively) that have termini at higher elevations (elevation ranges of 5000-5635 and 5195-5469 m a.s.l., respectively). The glaciers of the catchment were classified by Yang et al. (2013) as having a spring-accumulation regime and the longest rain season of the entire Tibetan Plateau. The upper Parlung River catchment has a mean summer (1979-2019) annual air temperature of ~2°C (at 4600 m a.s.l.), and temperatures in the wider region have been shown to be increasing since the mid 1990’s (Yang et al., 2013). The glaciers of this region have been shown to be very sensitive to temperature changes, though with a lower sensitivity of mass balance to elevation compared to other, continental glaciers of the Tibetan Plateau (Wang et al., 2019). Because Tibetan glaciers are shrinking and fragmenting, the accurate estimation of on-glacier temperatures is relevant for investigating and modelling their temperature sensitivity (Carturan et al., 2015). However, to date, no studies regarding the distribution of on-glacier temperature have been performed within the Tibetan Plateau.



161  
 162 *Figure 2: The location of Parlung catchment in Tibet (a) and a map of the Parlung glaciers (b) with the*  
 163 *study glaciers, Parlung 94 (c), Parlung4 (d) and Parlung390 (e). Off-glacier and on-glacier AWS and T-*  
 164 *Logger locations are shown (without glacier number suffix - see Table 1). (b) shows the elevation of the*  
 165 *catchment (DEM source: Alos Palsar) and (c-e) show the calculated flowline distances based upon*  
 166 *TopoToolbox (scales vary).*

167  
 168  
 169  
 170  
 171  
 172  
 173  
 174  
 175  
 176  
 177

### 3. Data

#### 3.1. Meteorological observations

We present the observations of  $T_a$  from a total of 20 air temperature logger locations (Table 1), 13 of which are situated on-glacier (4680 - 5369 m a.s.l.) and seven off-glacier (4648 - 5168 m a.s.l.). These stations (hereafter referred to as ‘T-loggers’) observed  $T_a$  at a 2 m height using HOBO U23-001 temperature-relative humidity sensors (accuracy  $\pm 0.21^\circ\text{C}$ ) within double-louvered, naturally-ventilated radiation shields (HOBO RS1) mounted on free-standing tripods. The T-loggers recorded data in 10 minute intervals that are averaged to hourly data for analysis. We identify a common observation period over the summers of 2018 and 2019 that ranges from

178 12<sup>th</sup> July – 18<sup>th</sup> September. For these date ranges, we observe only small data gaps for some T-  
 179 loggers (< 1% of the total period). We apply the nomenclature of  $TX_G$ , whereby  $X$  refers to the T-  
 180 logger number on each glacier and  $G$  refers to the glacier number (Table 1).

181

182

183 *Table 1: Details of each AWS/T-Logger station used in this analysis including the calculated flowline*  
 184 *distances.*

Station	Latitude	Longitude	Elevation (m a.s.l.)	Flowline (m)	on/off glacier
AWS_Off	29.314	96.955	4588	-	off
AWS_On	29.500	97.009	4808	-	off
T1 <sub>390</sub>	29.348	97.022	5095	-	off
T2 <sub>390</sub>	29.352	97.020	5168	-	off
T3 <sub>390</sub>	29.354	97.0202	5258	770	on
T4 <sub>390</sub>	29.356	97.020	5310	544	on
T5 <sub>390</sub>	29.357	97.019	5335	420	on
T6 <sub>390</sub>	29.359	97.018	5377	224	on
T1 <sub>94</sub>	29.621	97.218	4965	-	off
T2 <sub>94</sub>	29.417	96.99	4992	-	off
T3 <sub>94</sub>	29.635	96.975	5086	-	off
T4 <sub>94</sub>	29.596	97.065	5138	2481	on
T5 <sub>94</sub>	29.56	97.067	5174	2215	on
T6 <sub>94</sub>	29.466	97.023	5302	1411	on
T7 <sub>94</sub>	29.434	97.080	5280	1208	on
T8 <sub>94</sub>	29.399	97.097	5331	988	on
T1 <sub>4</sub>	29.271	96.968	4690	-	off
T2 <sub>4</sub>	29.368	96.935	4769	-	off
T3 <sub>4</sub>	29.298	97.168	4806	8589	on
T4 <sub>4</sub>	29.298	97.168	4809	7940	on
T5 <sub>4</sub>	29.496	97.126	4841	7505	on
T6 <sub>4</sub>	29.403	97.068	4909	6765	on

185

186

187 We additionally present  $T_a$  observations at two automatic weather stations (AWS) at elevations  
 188 ~4600 m a.s.l. (off-glacier, henceforth ‘AWS\_Off’) and ~4800 m a.s.l. (on Parlung4, henceforth  
 189 ‘AWS\_On’) for the same time period (Figure 2). The AWS  $T_a$  observations are provided by  
 190 Vaisala HMP60 temperature-relative humidity sensors (accuracy +0.5°C) housed in naturally-  
 191 ventilated, Campbell 41005-5 radiation shields. We obtain information regarding incoming  
 192 shortwave radiation and relative humidity (AWS\_Off), on-glacier wind speed (AWS\_On) and  
 193 ‘free-air’ wind speed and direction (ERA5 - C3S, 2017). We use these data to explore the  
 194 relationships of hourly on- and off-glacier temperatures (section 4.2) for different prevailing  
 195 conditions.

196

### 197 3.2. Intercomparison of air temperature observations

198 To evaluate the comparability of air temperature measurements, we calculate the hourly  
 199 divergence of two naturally-ventilated  $T_a$  observations for the whole period between T4<sub>4</sub> and  
 200 AWS\_On (Figure 2d), that are located within a few metres of horizontal distance of each other  
 201 on Parlung4 Glacier. A test of absolute differences between the two stations resulted in a mean of  
 202 < 0.4°C for all hours (n = 3312) and ~0.5°C for the warmest 10% of the hours of ambient

203 temperature at AWS\_Off. We find that for these warm hours (hereafter referred to as ‘P90’ -  
204 (Ayala et al., 2015; Shaw et al., 2017; Troxler et al., 2020)), when the *KBL* development is  
205 theoretically at its strongest (e.g. van den Broeke, 1997; Oerlemans and Grisogono, 2002), that  
206 95% of hourly differences were  $< 1^{\circ}\text{C}$  (Figure S1). For on-glacier stations at large flowline  
207 distances (Figure 2), large differences are considered less likely given the good ventilation  
208 provided to the sensors within the *KBL*. While observations at short flowline distances with calm  
209 conditions and high incoming radiation may result in larger differences up to  $\sim 1^{\circ}\text{C}$  (Troxler et al.,  
210 2020), we apply a  $\pm 0.5^{\circ}\text{C}$  ‘uncertainty’ for analysis of distributed  $T_a$ . For the instantaneous  
211 differences  $> 1^{\circ}\text{C}$ , wind speeds at AWS\_On were  $< 2\text{ m s}^{-1}$ . Wind speeds for P90 conditions were  
212 otherwise in excess of  $3\text{--}4\text{ m s}^{-1}$ , though no other observations of on-glacier wind speed are  
213 available at higher elevations. We note that in the absence of an artificially ventilated  $T_a$   
214 measurement as a reference (e.g. Georges and Kaser, 2002; Carturan et al., 2015), a true  
215 uncertainty value cannot be prescribed for the  $T_a$  observations of our study and only assumed  
216 based upon previous literature. This is discussed further in section 6.  
217

### 218 3.3. *Elevation information*

219 We use the 12.5 m Alos Palsar (ASF DAAC, 2020) digital elevation model (DEM) to obtain  
220 elevation information for the catchment (Figure 2b). Flowline distances (m) for each glacier are  
221 calculated from the TopoToolbox functions in Matlab (Schwanghart and Kuhn, 2010), following  
222 Troxler et al. (2020). We note that the methodology for flowline generation is not currently  
223 uniform among all studies of this type (Shea and Moore, 2010; Ayala et al., 2015; Carturan et al.,  
224 2015; Shaw et al., 2017; Bravo et al., 2019a; Troxler et al., 2020) and may produce some  
225 differences in the calculated distances close to the lateral borders of the glaciers. In addition, the  
226 generated flowlines may also be dependent upon the quality and resolution of the DEM  
227 available. However, we do not analyse lateral  $T_a$  variations in this study and consider the impact  
228 of varying methods for flowline generation to be negligible when assessing observations at a few  
229 selected points on the glacier.  
230

## 231 4. Methods

232 Our methods consist of (1) aggregating temperature observations based on off-glacier  
233 temperatures and prevailing meteorological conditions, (2) generating off-glacier temperature  
234 lapse rates to compare on and off-glacier temperatures at the same elevation, and (3) estimating  
235 the near-surface temperature sensitivity by fitting parameters to the model of Shea and Moore  
236 (2010). The following subsections outline the sub-grouping (4.1) and off-glacier  $T_a$  distribution  
237 (4.2) methodologies. The model parameterisations of Shea and Moore (2010) and application to  
238 Tibetan and global datasets are described in sections 4.3 and 4.4, respectively.

### 239 4.1. *Sub-grouping on-glacier air temperature observations*

240 Sub-grouping allows one to interpret general causal factors that dictate on-glacier behaviour. We  
241 sub-group our on-glacier observations by 10th and 90th percentiles (P10 = the coldest 10%, P90  
242 = the warmest 10%) of off-glacier  $T_a$  at AWS\_Off (Figure 2a). Following the methodology of  
243 previous studies (Ayala et al., 2015; Shaw et al., 2017; Troxler et al., 2020), we bin all  
244 contemporaneous observations of on-glacier  $T_a$  at each T-logger that correspond to the same hours  
245 as the coldest (P10) and warmest (P90) observations at AWS\_Off. We evaluate how strong the  
246 linear relationship of on-glacier  $T_a$  with elevation and flowline distance is for these subgroups  
247 using the coefficient of determination ( $R^2$ ). For a comparison to previous studies (Petersen and  
248 Pellicciotti, 2011; Shaw et al., 2017), we also report the equivalent on-glacier lapse rate that would  
249 be calculated for the above conditions.  
250

### 251 4.2. *Comparison of on- and off-glacier air temperature*

252 We extrapolate AWS\_Off  $T_a$  records to the elevation of each on-glacier T-logger (Table 1) to  
253 quantify the differences between ambient and on-glacier  $T_a$  (Figure 1a). We derive an hourly  
254 variable lapse rate between AWS\_Off and off-glacier T-loggers T1<sub>94</sub>, T2<sub>94</sub> and T1<sub>390</sub> to construct

255 a ‘catchment lapse rate’ where the origin of the calculated regression must pass through the  
 256 elevation of AWS\_Off (see supplementary information, Figure S2). These T-loggers are assumed  
 257 to be unaffected by the glacier boundary layer and we consider this as the best available approach  
 258 to estimate the ambient lapse rate for the catchment. We compare the hourly estimates of the  
 259 extrapolated off-glacier  $T_a$  ( $T_{aAmb}$ ) with the observations at each on-glacier T-logger in order to  
 260 i) quantify the differences and how they relate to meteorological conditions and glacier flowline  
 261 distance; and ii) parameterise the along flowline temperature sensitivity to  $T_{aAmb}$  following Shea  
 262 and Moore (2010) (section 4.3).

263

#### 264 4.3. Estimation of on-glacier temperature sensitivity

265

The Shea and Moore (2010) approach (hereafter ‘SM10’) estimates on-glacier  $T_a$  using  $T_{aAmb}$  at  
 266 a given elevation by:

267

$$268 \quad T_a = \begin{cases} T1 + k2(T_{aAmb} - T^*), & T_{aAmb} \geq T^* \\ T1 - k1(T^* - T_{aAmb}), & T_{aAmb} < T^* \end{cases}$$

269 (1)  
270

271 where  $T^*$  (°C) represents the threshold ambient temperature for the onset of katabatic flow and  
 272  $T1$  is the corresponding threshold  $T_a$  on the glacier. Parameters  $k1$  and  $k2$  are the temperature  
 273 sensitivities (ratio of on-glacier  $T_a$  to  $T_{aAmb}$ ) below and above the threshold  $T^*$  (Figure 1b and  
 274 c).  $k1$  and  $k2$  were parameterised in the original study using exponential functions of the along  
 275 flowline distance ( $DF$ ):

276

$$277 \quad k1 = \beta1 \exp(\beta2 DF)$$

278 (2)  
279

280

$$k2 = \beta3 + \beta4 \exp(\beta5 DF)$$

281

282 (3)  
283

284

where  $\beta_i$  are the fitted coefficients. Following the suggestion of Carturan et al. (2015), we  
 285 implement a relation against the flowline that estimates the threshold temperature for onset of  
 286 katabatic effects ( $T^*$ ) at a given distance as:

287

$$288 \quad T^* = \frac{C1DF}{C2 + DF}$$

289 (4)  
290

291 where  $C1$  (6.61) and  $C2$  (436.04) are the fitted coefficients of Carturan et al. (2015). We calculate  
 292  $k1$  and  $k2$  at each T-logger station using the linear regression of observed  $T_a$  and  $T_{aAmb}$  above  
 293 and below  $T^*$  (Figure 1) as derived from equation 4. We note that the parameter  $k2$  holds a greater  
 294 significance for modelling  $T_a$  (Figure 1a), as this more closely represents the ‘climatic sensitivity’  
 295 reported by previous works (Greuell et al., 1997; Greuell and Böhm, 1998; Oerlemans, 2001;  
 296 2010), whereas  $k1$  represents the ratio of above-glacier and free-air temperatures without a  
 297 katabatic effect that have been shown to relate more closely to  $T_{aAmb}$  (Shea and Moore, 2010;  
 298 Shaw et al., 2017). For this study, we therefore pay particular attention to the  $k2$  sensitivities on  
 299 the Parlung glaciers and assess their relationship to along-flowline distance.

300



#### 4.4. Global datasets of on-glacier temperatures

To explore the applicability of the SM10 approach and provide context to the findings of the Parlung catchment, we explore the calculated  $k1$  and  $k2$  parameters for several of the available distributed on-glacier datasets published to date (Figure S3, Table 2). We subset data for each glacier to those hours during the summer when all on-glacier observations were available. For sites of the Coastal Mountains of British Columbia ('CMBC' - Shea and Moore, 2010) and Alta Val de La Mare ('AVDM' - Carturan et al., 2015), we apply the published parameter sets derived from those authors. For all other sites, we derive  $T_a$  from the most locally available off-glacier AWS and the published lapse rate from the relevant studies (Table 2). In the absence of lapse rate information for a few glaciers, we apply the  $ELR$  ( $-6.5^\circ\text{C km}^{-1}$ ) to extrapolate  $T_a$  to the elevation of the on-glacier observations (see Table 2). We found that the calculation of  $k1$  and  $k2$  at those few glacier sites were not sensitive to the choice of lapse rate used, and varied  $< \pm 0.03$  for a  $\pm 1.5^\circ\text{C km}^{-1}$  change in the lapse rate.

For each glacier, the  $k1$  and  $k2$  parameters (equation 1) are only calculated when; i),  $>10\%$  of the total hourly data at a given station is above or below  $T^*$  (to have enough data to calculate  $k2$  and  $k1$ , respectively) and, ii) the linear regression to derive each parameter is significant to the 0.95 level. For those on-glacier stations that do not satisfy the above requirements, we do not calculate the  $k1$  and  $k2$  parameters.

Table 2: The details of each site where distributed on-glacier air temperatures are available. Elevation ranges and ERA5 mean summer air temperatures (MSAT) are reported for the year of investigation. Precipitation totals (mm - 'PT') were obtained from the cited literature.

Site	Lat	Lon	Year(s)	Elevation	MSAT <sup>a</sup>	PT	$T_a$ Data Reference
				m .a.s.l.	$^\circ\text{C}$	mm	
Parlung (Tibet)	29.24	96.93	2018-2019	4600-5800	2.19	679	This Study
CMBC (Canada)	50.32	-122.48	2006-2008	1375-2898	10.29	1113	Shea and Moore (2010)
AVDM (Italy)	46.42	10.62	2010-2011	2650-3769	7.94	1233 <sup>b</sup>	Carturan et al. (2015)
Tsanteleina (Italy)	45.48	7.06	2015	2800-3445	13.76	805	Shaw et al., (2017)
Arolla (Switzerland)	45.97	7.52	2010	2550-3520	7.28	1663	Ayala et al. (2015)
McCall (USA)	69.31	-143.85	2004-2014	1375-2365	-2.28	500	Troxler et al. (2020)
Juncal Norte (Chile)	-33.01	-70.09	2007-2008	2900-5910	6.58	352	Ayala et al. (2015)
Greve (Chile)	-48.88	-73.52	2015-2016	0-2400	-0.1	6450 <sup>c</sup>	Bravo et al. (2019a)
Pasterze (Austria)	47.09	12.71	1994	2150-3465	12.66	2761	Greuell and Böhm, (1998)
Universidad <sup>d</sup> (Chile)	-34.69	-70.33	2009-2010	2463-4543	8.24	474	Bravo et al. (2017)
Peyto <sup>d</sup> (Canada)	51.66	-116.55	2011	2260-3000	2.94	800	Pradhananga et al. (2020)
Djankuat <sup>d</sup> (Russia)	43.20	42.77	2017	3210-4000	12.13	950	Rets et al. (2019)

<sup>a</sup> MSAT corrected from ERA5 grid height to mean elevation of glacier using the environmental lapse rate

<sup>b</sup> Average for 1979-2009. Precipitation for 2010-2011 was above average at  $\sim 1400$  mm (L. Carutran, pers comm)

<sup>c</sup> Value taken from Bravo et al. (2019b)

<sup>d</sup> Glaciers where the ELR was used to distribute temperature for  $k1/k2$  calculation. See text for details.

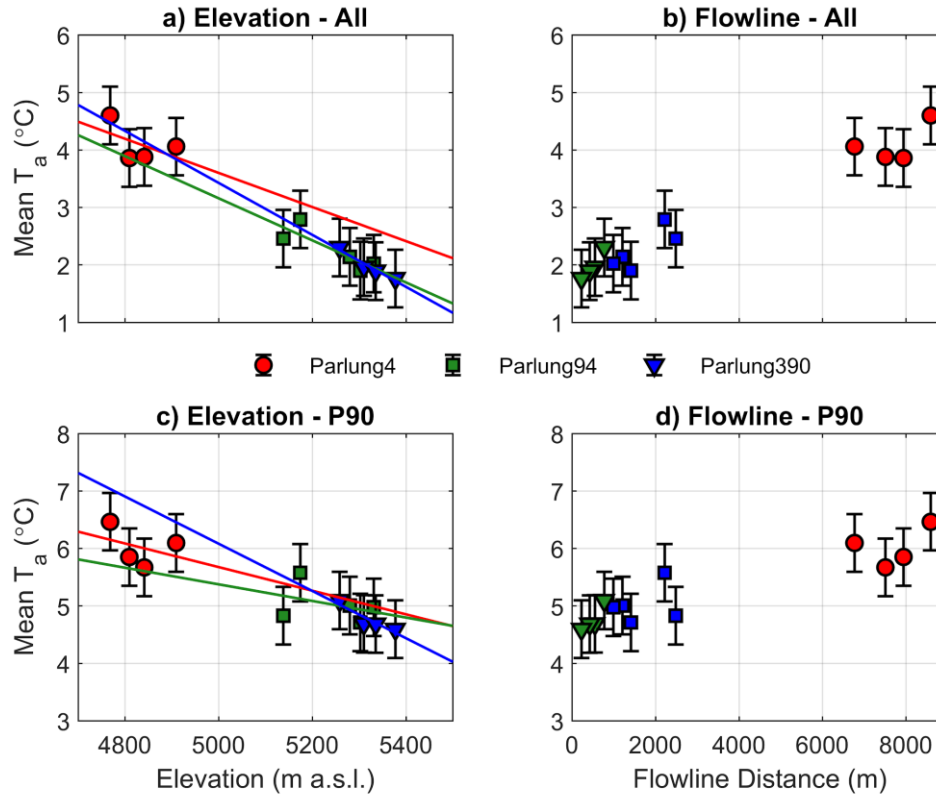
330  
331  
332  
333  
334  
335  
336  
337  
338  
339  
340  
341

Finally, we group the derived  $k_2$  sensitivities of the SM10 approach against the climatology that describes the given glacier(s) location. For this, we consider the mean summer (JJAS or DJFM in the southern hemisphere) air temperature (MSAT) and the total annual precipitation for the year(s) of study at each location (Table 2). MSAT is derived from the ERA5 product for the glacier centroid location and corrected to the mean glacier elevation by the *ELR*. However, total precipitation from ERA5 has been shown to have considerable bias when tested against in-situ observations (e.g. Betts et al., 2019), and so we provide the best available value from the relevant literature (Table 2). We note that a full analysis of the local climate is beyond the scope of this work, though we attempted a generalised analysis in order to link any clear differences in the global datasets to climatological influences.

## 342 **5. Results**

### 343 *5.1. Variability of on-glacier air temperatures*

344 Figure 3 shows the mean  $T_a$  as a function of elevation and flowline distance for the Parlung  
345 glaciers for all conditions and for the warmest 10% of AWS\_Off observations (P90). The average  
346 of all hours ( $n = 3312$ ) reveals a generally linear relationship with the glacier elevation (Figure  
347 3a) and flowline distance (Figure 3b), resulting in mean on-glacier lapse rate (mean  $R^2$  with  
348 elevation) equivalent to  $-3.0^\circ\text{C km}^{-1}$  (0.92),  $-3.7^\circ\text{C km}^{-1}$  (0.71) and  $-4.5^\circ\text{C km}^{-1}$  (0.81) for  
349 Parlung4, Parlung94 and Parlung390, respectively. For P90 hours ( $n = 312$ ), mean  $T_a$   
350 demonstrates a poorer fit to elevation and with flowline distance for Parlung4 (mean  $R^2$  with  
351 elevation = 0.12, and flowline = 0.20) and Parlung 94 (mean  $R^2$  with elevation = 0.13 and flowline  
352 = 0.09). For the small Parlung390 Glacier,  $T_a$  remains strongly related to elevation ( $R^2 = 0.84$ )  
353 and flowline ( $R^2 = 0.82$ ) under P90 conditions. The equivalent mean on-glacier ‘lapse rates’ for  
354 P90 hours are  $-2.1^\circ\text{C km}^{-1}$ ,  $-1.4^\circ\text{C km}^{-1}$  and  $-4.1^\circ\text{C km}^{-1}$ . Nevertheless, assuming a  $0.5^\circ\text{C}$   
355 uncertainty of the observations for P90 conditions (Figure 3c and d), the mean of observations  
356 still lies along a linear fit line. However, for given hours, the deviation of observations from the  
357 linear fit line exceeds  $3^\circ\text{C}$  at large flowline distances ( $> 7000$  m) on Parlung4. In general, 2018  
358 experienced cooler average temperatures at higher elevations, but in general, there are no marked  
359 differences between the two years of observation when comparing on-glacier  $T_a$  to glacier  
360 elevation or flowline (not shown).  
361



362  
 363 *Figure 3: The mean  $T_a$  against elevation and uncertainty (errorbar) for (a) all hours ( $n = 3312$ ) and (c)*  
 364 *P90 hours ( $n = 312$ ). Panels (b) and (d) are the equivalent plots against flowline distance. Coloured lines*  
 365 *show the linear fit against elevation ('lapse rate') to each glacier.*

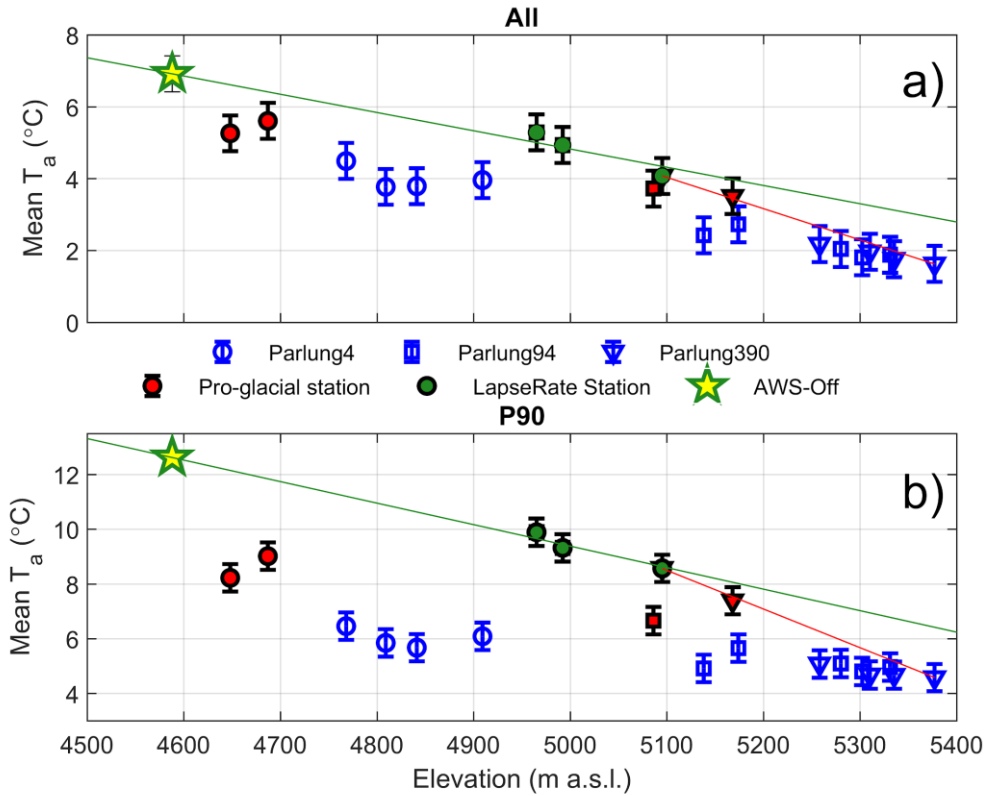
366

367

### 368 5.2. Differences in on- and off-glacier air temperatures

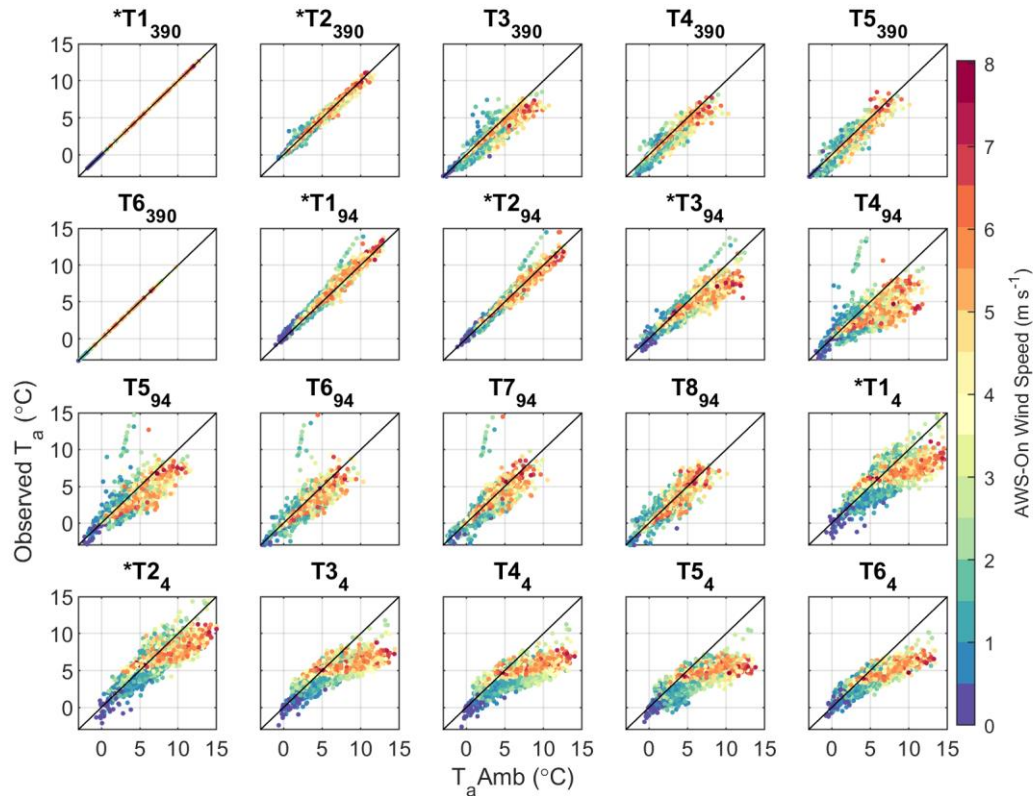
369 Comparing mean on- and off-glacier  $T_a$  at the same elevation reveals the expected behaviour  
 370 associated with the glacier 'cooling effect' (Carturan et al., 2015) and a greater deviation from  
 371 the calculated catchment lapse rate temperature for the warmest conditions (P90, Figure 4),  
 372 indicating a reduced temperature sensitivity. The mean  $T_a$  observed at off-glacier T-Loggers  
 373 supports the selection of those stations used for catchment lapse rate calculation (green dots in  
 374 Figure 4) that are further from the potential effects of the glacier boundary layer (red markers in  
 375 Figure 4). Following Carturan et al. (2015), we suggest a potential non-linear behaviour of lapse  
 376 rates between AWS\_Off and the top of the flowline for Parlung390, though we lack the off-glacier  
 377 observations above the flowline origin to test this (Figure 4b). We therefore utilise a piecewise  
 378 lapse rate at the point of the highest off-glacier lapse rate station (T1<sub>390</sub> - red line in Figure 4) to  
 379 account for the discrepancy between the estimated and observed  $T_a$  at T6<sub>390</sub>, which is assumed to  
 380 be near to the flowline origin where temperature sensitivity is theoretically equal to 1 (i.e. where  
 381 the on-glacier observations are expected to match  $T_{aAmb}$ ).

382



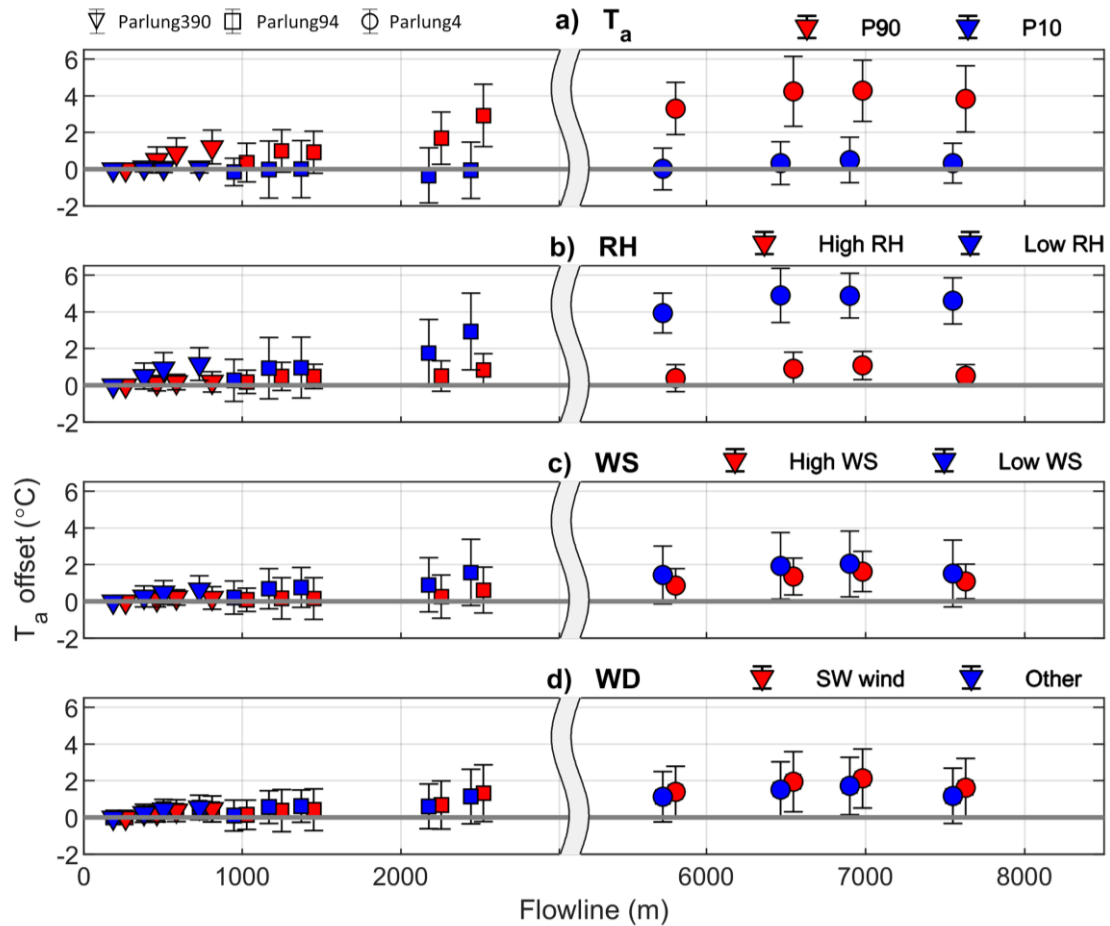
383  
 384 *Figure 4: The mean  $T_a$  against elevation for all hours (a) and P90 hours (b), where blue markers are on-*  
 385 *glacier T-Loggers, red markers are pro-glacial T-Loggers and green circles denote off-glacier T-Loggers*  
 386 *used to construct an hourly variable ‘catchment lapse rate’ (green line), extrapolated from AWS\_Off*  
 387 *(star). The red line indicates the piecewise lapse rate above the elevation of  $T1_{390}$  to lapse  $T_a$  to the top of*  
 388 *the flowline. A  $0.5^\circ\text{C}$  uncertainty is shown by the errorbar for each station (not applied to the lapse rate*  
 389 *for neatness).*

390  
 391  
 392 Figure 5 presents the hourly differences between  $T_a\text{Amb}$  and observed  $T_a$  at each site. The  
 393 deviation of estimated and observed  $T_a$  theoretically begins at a critical temperature threshold,  $T^*$   
 394 (Shea and Moore, 2010) and this effect can be observed at T-logger sites on Parlung94 and  
 395 Parlung4, particularly those at greater flowline distances. On-glacier  $T_a$  and  $T_a\text{Amb}$  align well  
 396 until the onset of katabatic winds (on Parlung4 and only assumed for the other glaciers due to lack  
 397 of on-glacier wind observations – Figure 5). Despite being pro-glacial stations,  $T1_4$  and  $T2_4$  reveal  
 398 a similar, albeit weaker effect of the glacier boundary layer, possibly due to larger glacier flowline  
 399 and extension of the katabatic wind into the pro-glacial area.  
 400



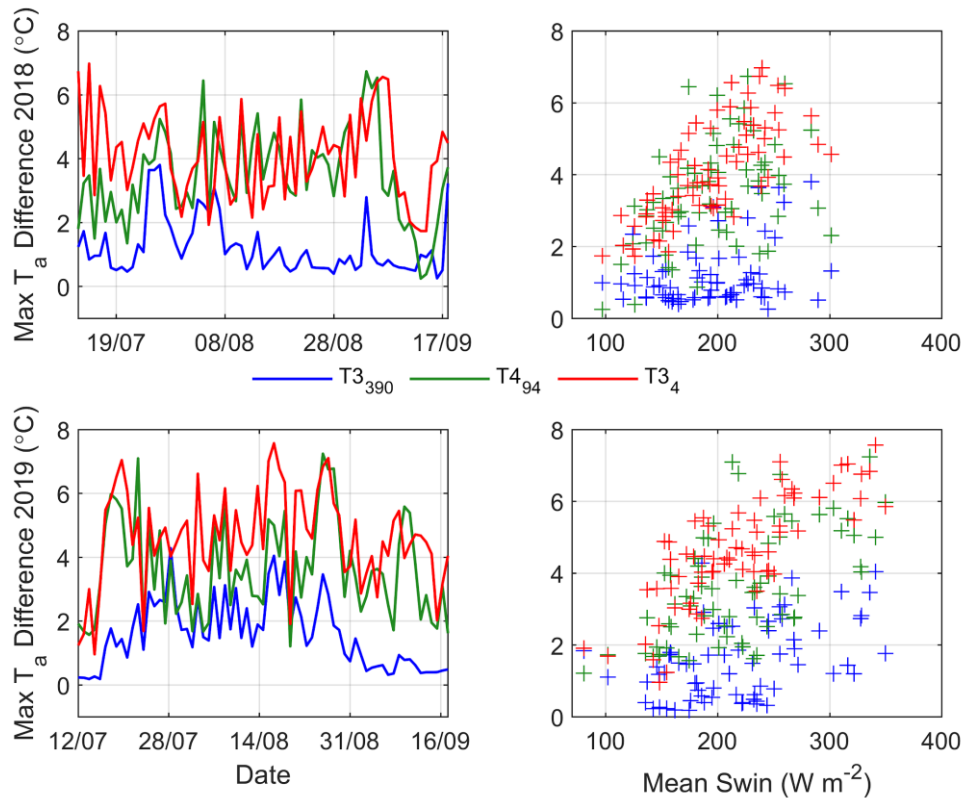
401  
 402 *Figure 5: Estimated ( $T_{aAmb}$ ) vs Observed  $T_a$  at each T-Logger location (including off-glacier T-*  
 403 *Loggers). Individual, hourly values are coloured by the observed wind speeds at AWS\_On (Parlung4). \**  
 404 *denotes stations that are off-glacier.*  
 405

406  
 407 The mean difference of along-flowline  $T_a$  and  $T_{aAmb}$  using the catchment lapse rate is shown in  
 408 Figure 6. For the coolest 10% of hours at AWS\_Off (P10), there is generally minimal difference  
 409 between  $T_{aAmb}$  and observed  $T_a$  for the entire dataset. For P90 conditions (Figure 6a), differences  
 410 between  $T_{aAmb}$  and observed on-glacier temperatures are up to 5.8 C at flowline distances greater  
 411 than 7000 m. These differences appear to increase beyond 2000 m along the flowline (Parlung94),  
 412 though significant differences can be witnessed for all glaciers (different symbols in Figure 6).  
 413 This is generally associated with drier conditions, and for hours of greater relative humidity  
 414 (AWS\_Off), when conditions are generally cooler, differences are unsurprisingly smaller (Figure  
 415 6b). Considering ‘free-air’ wind variability provided by ERA5 reanalysis,  $T_a$  differences are  
 416 largest for the dominant south-westerly wind direction (85% of hours) and when free-air wind  
 417 speeds are smallest (Figure 6c and 6d). However, un-corrected, gridded wind speeds do not  
 418 appropriately represent the local ‘free-air’ boundary conditions and thus the interaction of off-  
 419 glacier wind speeds and the glacier boundary layer development remain unclear for these glaciers.  
 420 For all but the coolest ambient temperatures (Figure 6a), observations at the greatest flowline  
 421 distances deviate the most from the estimated values. Besides the analyses against individual  
 422 meteorological variables, the differences are largest for warm/anticyclonic conditions, and lowest  
 423 for cool/cyclonic conditions.  
 424



425  
 426 *Figure 6: The mean and standard deviation (error-bars) of hourly  $T_a$  differences ( $T_{aAmb}$  - observed)*  
 427 *along the glacier flowline. Each panel depicts hourly grouping by (a) off-glacier  $T_a$  at  $AWS\_Off$  ( $P90 \geq$*   
 428  *$10.5^\circ\text{C}$  and  $P10$  is  $\leq 3.5^\circ\text{C}$ ), (b) off-glacier RH at  $AWS\_Off$  (high is  $> 90\%$  and low is  $< 70\%$ ), (c)*  
 429 *wind speed from ERA5 (high is  $> 2.5 \text{ m s}^{-1}$  and low is  $< 0.7 \text{ m s}^{-1}$ ) and (d) dominant wind direction from ERA5*  
 430 *(Southwest wind direction is considered as  $180\text{-}270^\circ$ ). Marker shapes show the different glaciers, as in*  
 431 *Figure 3 and 4. X axes are split to improve visibility at low flowline distances.*  
 432  
 433

434 The differences between  $T_{aAmb}$  and on-glacier  $T_a$  are highly variable in time, however, and  
 435 related to the prevailing conditions of a given year (Figure 7). Considering the maximum daily  $T_a$   
 436 differences at the on-glacier T-Logger closest to the terminus of each glacier (Table 1, Figure 2),  
 437 we find that Parlung94 and Parlung4 T-loggers have similar magnitudes of  $T_a$  offsets during the  
 438 mid-summer months, particularly for 2018 (Figure 7). These maximum differences are in clear  
 439 relation to the incoming shortwave radiation recorded at  $AWS\_Off$  (correlations of 0.44, 0.60 and  
 440 0.80 for Parlung390, Parlung94 and Parlung4, respectively), which are indicative of warmer  
 441 ambient conditions (i.e. P90). For Parlung390 the maximum daily differences are much smaller,  
 442 though they vary considerably throughout the summer. For 2019, maximum daily  $T_a$  offsets on  
 443 Parlung390 steadily increase during July and August then fall close to zero in September. The  
 444 maximum differences for Parlung4 and Parlung94, however, remain sizeable (Figure 7), perhaps  
 445 due to the persistence of katabatic winds over a larger flowline distance even under the relatively  
 446 cooler conditions of September. Because our study period focuses on the core monsoon period  
 447 (Yang et al., 2011), we do not observe the influence of monsoon arrival or cessation on the  $T_a$   
 448 variability of the Parlung Glaciers.  
 449



450

451 *Figure 7: Maximum daily  $T_a$  differences ( $T_{aAmb}$  - observed) at the T-Logger closest to the terminus on*  
 452 *each glacier for 2018 (top panels) and 2019 (bottom panels). Maximum daily  $T_a$  differences are plotted*  
 453 *against mean daily incoming shortwave radiation at AWS\_Off in the right hand panels.*

454

455

456

### 5.3. Parameterisation of along-flowline air temperatures

457

458

459

460

461

462

463

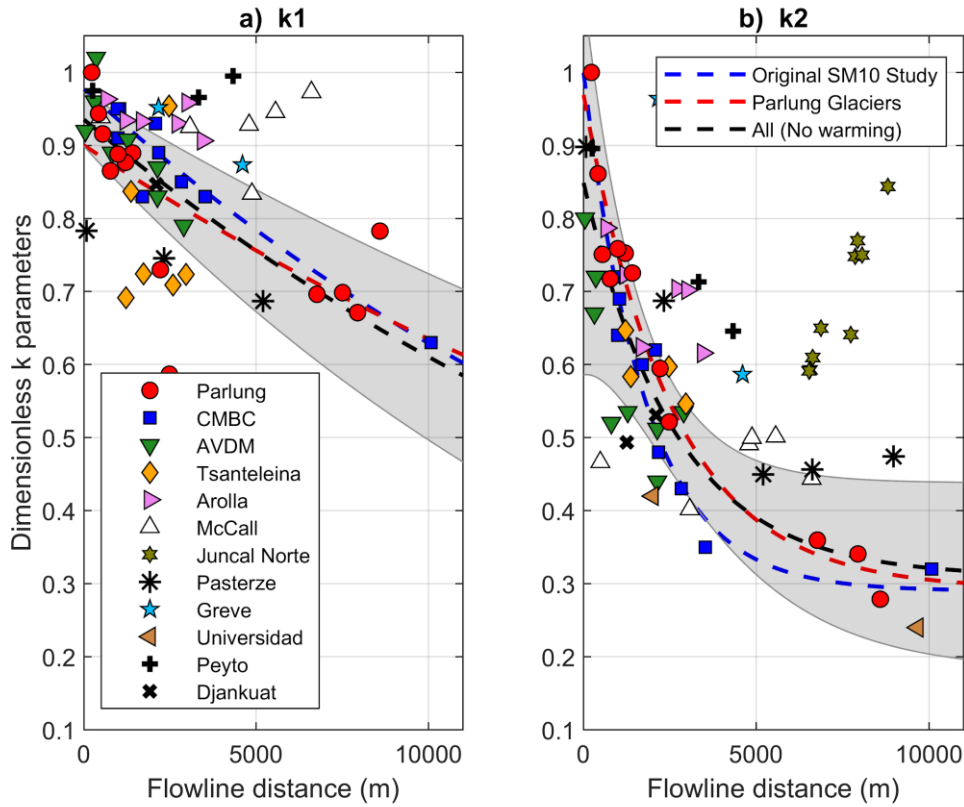
464

465

466

467

Figure 8 presents the temperature sensitivities of the SM10 approach for the Parlung glaciers and available distributed  $T_a$  datasets around the world (Table 2). Comparing the  $k1$  and  $k2$  parameters from Tibet to the parameters of Shea and Moore (2010) from western Canada, a similar behaviour is observable up to  $\sim 2000$ - $3000$  m of flowline distance (red and blue symbols). The exponential functions that are fitted to the observations at Parlung glaciers and the original study are distinct (red and blue lines in Figure 8, Table 3), although within the confidence intervals of each other. Fitting an exponential function for all sites where a down-glacier decrease in temperature sensitivity ( $k2$ ) is evident (black dashed line in Figure 8b) clearly misrepresents many of the observations, particularly those at greater flowline distances, balancing the behaviours reported for different sites.



468

469 *Figure 8: The calculated  $k1$  and  $k2$  sensitivities as a function of the flowline distance of each observation*  
 470 *on the Parlung glaciers (red circles) and other, global datasets (Table 2). The dashed blue and red lines*  
 471 *show the fitted exponential parameterisation of Shea and Moore (2010) and this study, respectively. The*  
 472 *dashed black line and shaded area denotes the equivalent parameterisation for all observations without a*  
 473 *large increase in sensitivity on the glacier terminus ('warming effect' - explicitly excluding data from*  
 474 *McCall, Juncal Norte and Djankuat). The shaded area represents the 95% confidence interval of this fit*  
 475 *line.*

476

477

478 *Table 3: The coefficients of the original SM10 model and those fitted to the  $k1$  and  $k2$  sensitivities on the*  
 479 *Parlung glaciers and all glaciers where no warming effect was evident (see Figure 10).*

Model	$k1 = \beta1 * \exp(\beta2 * DF)$	$k2 = \beta3 + \beta4 * \exp(-\beta5 * DF)$
CMBC (Shea and Moore, 2010)	$\beta1 = 0.977$ $\beta2 = -4.4e-5$	$\beta3 = 0.29$ $\beta4 = 0.71$ $\beta5 = 5.6e-3$
Parlung	$\beta1 = 0.894$ (0.805,0.983) $\beta2 = -2.972e-5$ (-5.543e-5,-4.0e-6)	$\beta3 = 0.349$ (0.241,0.456) $\beta4 = 0.624$ (0.492,0.757) $\beta5 = 4.4e-3$ (1.7e-4,7.2e-4)
All (no increased sensitivity on glacier terminus)	$\beta1 = 0.923$ (0.886,0.96) $\beta2 = -3.375e-5$ (-5.543e-5,-4.0e-6)	$\beta3 = 0.343$ (0.225,0.46) $\beta4 = 0.511$ (0.38,0.642) $\beta5 = 4.2e-3$ (1.5e-4,6.9e-4)

480

481

482 Notably, observations at McCall Glacier, Alaska relate very well to ambient  $T_a$  under cooler  
 483 conditions, with most  $k1$  values remaining  $> 0.9$ . Above the  $T^*$  threshold, however, the  
 484 relationship of observed and estimated  $T_a$  results in increasing  $k2$  along the flowline, in  
 485 contradiction to the majority of the other datasets. Nevertheless, this data also confirms the  
 486 increased temperature sensitivity on the glacier terminus (Troxler et al., 2020) as evident with



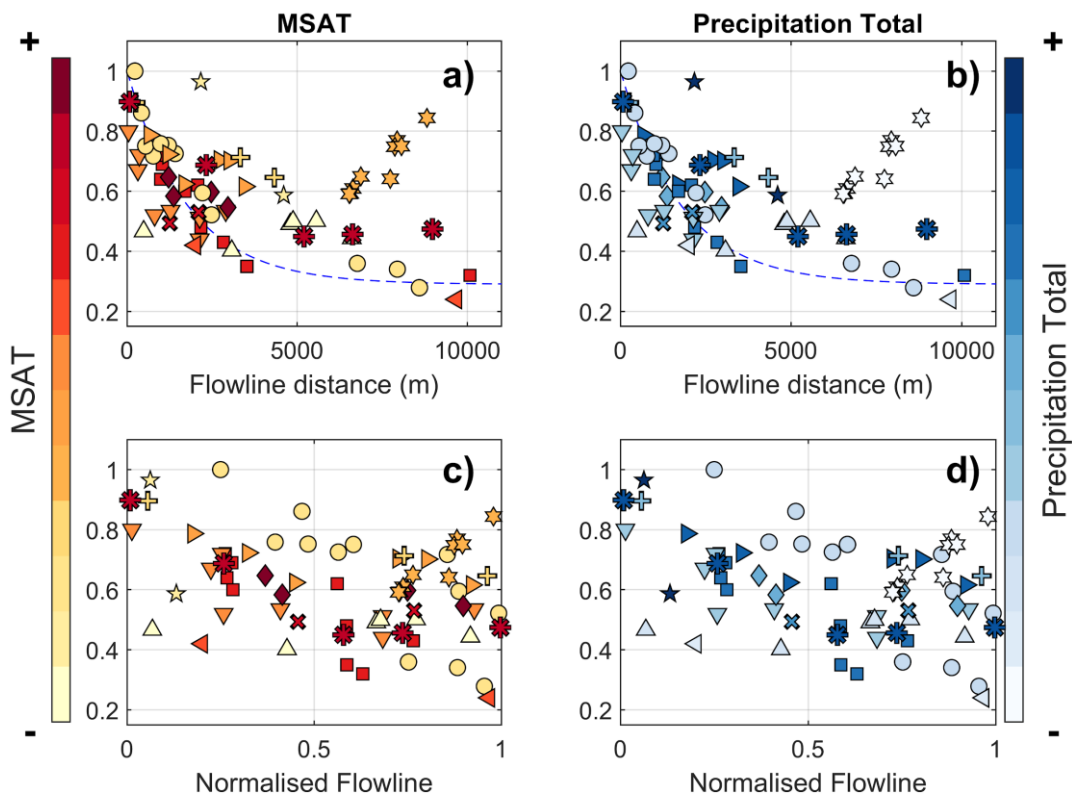
487 datasets for Tsanteleina (Shaw et al., 2017), Arolla and Juncal Norte (Ayala et al., 2015).  
 488 Observations at Parlung4 and Universidad Glacier (Bravo et al., 2017) emphasise the strong  
 489 decrease in temperature sensitivity at large flowline distances ( $\sim 10,000$  m) previously only  
 490 witnessed from one location on Bridge Glacier, Canada (Shea and Moore, 2010). At these  
 491 stations, changes in on-glacier  $T_a$  are less than a third of the equivalent change in  $T_{aAmb}$ .

492

493 Figure 9 shows the  $k_2$  parameters plotted against flowline distance, coloured by rankings of  
 494 MSAT and precipitation totals (Table 2). The warmest of the investigated sites (during the  
 495 measurement years) lie closer to the original SM10 exponential function up to  $\sim 4000$  m, whereas  
 496 deviation of the  $k_2$  parameters from this line appears larger for the relatively cold sites (Greve,  
 497 McCall and Peyto – Figure 9a). The main exception to this is for Juncal Norte, which  
 498 demonstrates a high and rapidly increasing sensitivity of ambient  $T_a$  at the greatest flowline  
 499 distances.

500 No clear patterns are visible in relation to mean annual precipitation, though the distinct behaviour  
 501 at Juncal Norte Glacier corresponds to the driest of the study sites considered (Figure 9b).  
 502

502



503

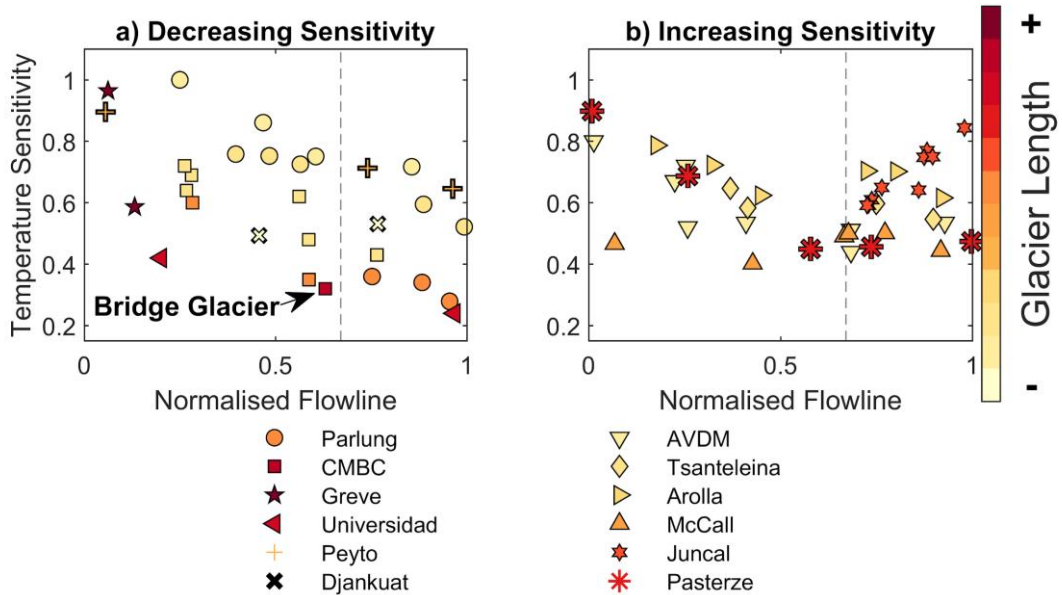
504 *Figure 9: The  $k_2$  sensitivities as a function of flowline distance (top) and a normalized distance, considering*  
 505 *the total flowline distance for the year of study (bottom). The individual glaciers of grouped studies*  
 506 *(Parlung, CMBC and AVDM) are separated and normalized by the individual glacier length (symbols as*  
 507 *in Figure 8). Glaciers are coloured by rankings of the mean summer air temperatures (MSAT - left) and*  
 508 *precipitation total (right). The original SM10 parameterisation is retained in the top panels.*

509

510

511 A clear difference between the station observations of Shea and Moore (2010) and Parlung  
 512 glaciers at large flowline distances (Figure 8) is the total distance of that station observation from  
 513 the glacier terminus, which suggests a possible difference in processes occurring between sites.  
 514 Accordingly, we plot the  $k_2$  parameters as a function of the normalised flowline (Fig 9c and d),  
 515 adjusted by the total length of glacier for the year(s) of observation (Table 2). The largest flowline  
 516 distance observation of the entire dataset (Figure 9a) extends only  $\sim 60\%$  of the total glacier length  
 517 (Bridge Glacier - CMBC), neither representing the smallest temperature sensitivity (Figure 8b),

518 nor an increasing temperature sensitivity witnessed at the terminus of the glacier (and estimated  
 519 using the ModGB model) by other studies (Ayala et al., 2015; Troxler et al., 2020). We group  
 520 glaciers by the presence (or absence) of an increasing temperature sensitivity on the terminus in  
 521 Figure 10. We find that there is no clear relation between the total length of the glacier and  
 522 increasing temperature sensitivity, which is seen for both smaller and larger glaciers (Figure 10b).  
 523 For those glaciers where a temperature sensitivity increase (a relative ‘ModGB’ warming effect -  
 524 Figure 1a) is evident, it is found only on the lowest 30% of the glacier terminus (Figure 10b –  
 525 vertical dashed line).  
 526



527  
 528 *Figure 10: The  $k_2$  sensitivity along the normalized flowline compared to total glacier length (colour bar).*  
 529 *Glaciers have been grouped in two clusters: a) those with down-glacier decreasing sensitivity, and b) those*  
 530 *with increasing sensitivity towards the glacier terminus.*

531  
 532

## 533 6. Discussion

### 534 6.1. Relevance of the findings from Parlung Glaciers

535 Our observations of along-flowline  $T_a$  on the glaciers in the Parlung catchment provide more  
 536 evidence of the spatial variability of the glacier cooling and dampening effect (Oerlemans, 2001;  
 537 Carturan et al., 2015; Shaw et al., 2017) and highlights the need to appropriately estimate its  
 538 behaviour for use in glacier energy balance and enhanced temperature index melt models  
 539 (Petersen and Pellicciotti, 2011; Shaw et al., 2017; Bravo et al., 2019a). It has long been observed  
 540 that a static lapse rate is inappropriate for characterising the spatio-temporal variability of  $T_a$ , both  
 541 within the *KBL* (Greuell et al., 1997; Konya et al., 2007; Marshall et al., 2007; Gardner et al.,  
 542 2009; Petersen and Pellicciotti, 2011) and outside the glacier boundary layer in adjacent valleys  
 543 (Minder et al., 2010; Immerzeel et al., 2014; Gabbi et al., 2014; Heynen et al., 2016; Jobst et al.,  
 544 2016). Despite this, the lack of locally available observations often requires modellers to force  
 545 models with the nearest off-glacier record of  $T_a$  and extrapolate it based upon the *ELR* value as a  
 546 default. In the case of Tibetan glaciers, model studies have often derived static lapse rates between  
 547 on-and off-glacier stations (Huintjes et al., 2015) or downscale  $T_a$  with a correction factor based  
 548 upon a single on-glacier location (e.g. Caidong and Sorteberg, 2010; Yang et al., 2013; Zhao et  
 549 al., 2014). To the authors’ knowledge, this is the first time that such detailed information regarding  
 550 spatio-temporal variations in  $T_a$  have been presented for a glacier of the Tibetan Plateau. Because  
 551 glaciers of the south-eastern Tibetan Plateau have been shown to be particularly susceptible to  
 552 increases in  $T_a$  (Wang et al., 2019), accurately parameterising  $T_a$  along glaciers of differing size  
 553 is highly relevant for present and future melt modelling attempts. This is especially true where

554 glaciers begin to shrink or fragment (Munro and Marosz-Wantuch, 2009; Jiskoot and Mueller,  
555 2012; Carturan et al., 2015) and become more sensitive to ambient air temperatures due to a lack  
556 of katabatic boundary layer development (Figures 6 and 7).

557

558 The summer monsoon exerts a strong control on the energy and mass balance of Tibetan glaciers  
559 (Yang et al., 2011; Mölg et al., 2012; Zhu et al., 2015). Although our dataset spanned two  
560 summers of only the core monsoon period for this region (Yang et al., 2011), we have shown that  
561 the sensitivity of the glacier to external temperature changes (shown by on-glacier and ambient  
562  $T_a$  differences) has a sizeable temporal variability that can be controlled by the monsoon weather  
563 conditions (such as ambient air temperature, humidity and incoming radiation) and can sometimes  
564 be independent of the glacier size (Figure 7). Whilst we cannot determine the impact of monsoon  
565 timing and intensity upon the temperature sensitivity of these glaciers with the current dataset, we  
566 are able to determine that the observed relationship to flowline distance is consistent to that of  
567 other regions of the world (Figure 8). Future work on Tibetan glaciers should attempt to extend  
568 monitoring to the pre-monsoon period to identify if a seasonal onset for the changing glacier  
569 temperature sensitivity can be defined, and how the monsoon may affect it. Particular focus  
570 should be given to understand the local meteorological conditions for each glacier, as this may  
571 explain some of the variability in  $T_a$  offset values, and why they may sometimes be independent  
572 of the along-flowline distance (Figure 7).

573

574

## 6.2. *Parameterising glacier temperature sensitivity*

575

576 In this study, we discuss the temperature sensitivity of on-glacier  $T_a$  based upon observations  
577 above a threshold ambient temperature for the onset of katabatic conditions ( $T^*$ ). This sensitivity  
578 to ambient temperature during relatively warm conditions, indicated by the  $k_2$  parameter of Shea  
579 and Moore (2010)(Figure 1), demonstrates a generally consistent behaviour between the T-logger  
580 observations of Parlung glaciers and those where this model had been previously implemented  
581 (Shea and Moore, 2010; Carturan et al., 2015). While data from the Parlung catchment provides  
582 an important confirmation of the temperature sensitivity for some Tibetan glaciers, further studies  
583 of individual glaciers can provide only local parameterisations for temperature sensitivity that  
584 may not be applicable to other sites. Accordingly, we have made here one of the first attempts at  
585 combining many of the published datasets regarding distributed  $T_a$  on mountain glaciers around  
586 the world (Table 2) to examine the potential transferability of a model accounting for temperature  
587 sensitivity (Figure 8).

587

588 We found a sizeable spread in the temperature sensitivities of  $T_a$  for the on-glacier datasets  
589 considered, though a consistently rapid decrease of sensitivity along glacier flowlines is found for  
590 most sites up until ~2000-3000 m of distance (Figure 8b). While localised meteorological and  
591 topographic factors likely interact to explain the spread of sensitivities at small flowline distances  
592 (Figure 8b), the results suggest that small glaciers with flow lengths < 1000 m would reflect a  
593 0.7-0.8 sensitivity to changes in  $T_{aAmb}$ . Beyond this distance, the temperature sensitivities  
594 notably follow one of two patterns; a continued, albeit less rapid decrease in sensitivity (generally  
595 following the model proposed by Shea and Moore (2010)), or a tendency toward increasing  
596 sensitivity at the largest flowline distances (in agreement with the ‘ModGB’ model - Figure 1a).  
597 With reference to the relative  $T_a$  differences among only on-glacier observations, these have been  
598 termed as down-glacier ‘cooling’ or ‘warming’, respectively for many past studies (Ayala et al.,  
599 2015; Carturan et al., 2015; Shaw et al., 2017; Troxler et al., 2020). Whilst the former is generally  
600 associated with relatively warmer regions of study (Figure 9), such as the southern Coast  
601 Mountains (Shea and Moore, 2010) or Universidad Glacier (Bravo et al., 2017), no strong  
602 relationship of the climate setting exists between these sites to explain the magnitude of the  
603 temperature sensitivity (i.e. the strength of the glacier cooling and dampening effect) nor the  
604 observed increases in temperature sensitivity on glacier termini (Ayala et al., 2015; Shaw et al.,  
605 2017; Troxler et al., 2020).

606

607 Interestingly, we noted that the station with the largest flowline distance used to derive the  
608 parameterisation by Shea and Moore (2010) was located only around 60% of the total glacier

609 flowline distance (Bridge Glacier - Figure 10), whereas data presented by other studies, provided  
610 observations up to the glacier terminus (Greuell and Böhm, 1998; Ayala et al., 2015; Shaw et al.,  
611 2017; Troxler et al., 2020), therefore potentially parameterising different effects of the glacier  
612 boundary layer. It has been suggested that observations at large flowline distances (such as that  
613 on Parlung4 or Bridge Glacier) represent a segment of the boundary layer where the near-surface  
614 layer becomes highly insensitive to the ambient free-air temperature fluctuations (point '3' in  
615 Figure 1a and d). This phenomenon has been shown to be sustained over large fetch distances by  
616 an increasing depth of the glacier wind layer (van den Broeke et al., 1997; Greuell and Böhm,  
617 1998; Shea and Moore, 2010, Jiskoot and Mueller, 2012). However, as air parcels travel down-  
618 glacier toward the glacier terminus (point '4' in Figure 1a and d), they potentially encounter warm  
619 air entrainment due to a divergent boundary layer (Munro, 2006), up-valley winds (Pellicciotti  
620 et al., 2008; Oerlemans, 2010; Petersen and Pellicciotti, 2011), large changes in surface slope and  
621 the dominance of adiabatic heating over sensible heat losses (Greuell and Böhm, 1998) or heating  
622 from debris-covered ice at the terminus (Brock et al., 2010; Shaw et al., 2016; Steiner and  
623 Pellicciotti, 2016; Bonekamp et al., 2020). These are effects of the glacier boundary layer that the  
624 ModGB model was designed to account for, though we did not explicitly test this within our study  
625 due to a requirement for more data and a greater number of parameters and assumptions (Shaw et  
626 al., 2017). The strength of this so called along-glacier 'warming effect' could therefore be  
627 governed by local topography (adjusting the boundary layer convergence or divergence) or the  
628 total glacier flowline distance and the large fetch of a cool air parcel overcoming the competing  
629 effect of warm, up-valley winds (Figure 1d - as seen at T<sub>24</sub> in Figure 5).

630

631 By grouping glaciers by the presence of the observed increase in temperature sensitivity and  
632 normalising the flowline distance of the observations by the total flowline for each glacier, we  
633 identify that the relative increases in temperature sensitivity begin at ~ 70% of the total flowline  
634 distance (Figure 10). A smaller temperature sensitivity can be observed for larger glaciers (Figure  
635 10a), which is consistent with the development of the *KBL* over a large fetch (Greuell and Böhm,  
636 1998; Shea and Moore, 2010), though the length itself indicates nothing clear about why greater  
637 temperature sensitivity exists for some glacier termini (Figure 10b).

638

639 The clear outlier of these datasets is Juncal Norte Glacier in Chile (Figure 8b). It is interesting to  
640 note that Juncal Norte is the only reported case in the literature on  $T_a$  variability where the warmest  
641 hours of the afternoon correspond to the dominance of an up-valley, off-glacier wind (Pellicciotti  
642 et al., 2008; Petersen and Pellicciotti, 2011). Counter to the typical role of the dominant, down-  
643 glacier wind layer for these warmest afternoon hours (Greuell et al., 1997; Greuell and Böhm,  
644 1998; Strasser et al., 2004; Jiskoot and Mueller, 2012; Shaw et al., 2017; Troxler et al., 2020), up-  
645 valley winds on Juncal Norte seemingly erode the along-flowline reduction in temperature  
646 sensitivity (along-flowline cooling) up to a distance along the flowline where it is theoretically at  
647 its maximum (point '3' in Figure 1). Evidence from other glaciers suggest that this point is close  
648 to upper observations for Juncal Norte at ~70% of the total flowline (Figure 10b), though further  
649 observations on Juncal Norte Glacier would be required to test this.

650

651 Finally, the extent to which a glacier terminus is constrained by high valley slopes may be an  
652 additional explanatory factor for the occurrence of increasing temperature sensitivities on some  
653 glaciers (Figure 10). While this may limit the suggested boundary layer divergence (Munro,  
654 2006), it may equally promote greater warming due longwave emission from valley slopes (e.g.  
655 Strasser et al., 2004; Ayala et al., 2015). We calculated the terminus width/ length ratio of each  
656 glacier and compared it to the presence of increasing temperature sensitivity on the terminus  
657 (supplementary Figure S4), revealing a potential relationship between the two. However, given  
658 the available data for this study and the unknown extent to which longwave emission may affect  
659 a fast-moving air parcel (Ayala et al., 2015), a dedicated study would be required to further  
660 address this hypothesis.

661

662

### 6.3. Future directions for researching air temperatures on glaciers

663 A limitation of our work is the dependency of the derived ‘global’ temperature sensitivities  
664 (Figure 8b) to the available off-glacier data and the published lapse rates to extrapolate them to  
665 the relevant elevations on-glacier. In our case, we are able to identify a potentially non-linear  
666 lapse rate of  $T_a^{Amb}$  for the highest elevations over Parlung94 and Parlung390 (Figure 4).  
667 Although we cannot confirm this without off-glacier observations above the top of the flowline  
668 (Carturan et al., 2015), we are able to well constrain ambient air temperature distribution using  
669 hourly observations at several off-glacier locations to derive the best possible ‘catchment lapse  
670 rate’. For other datasets (Table 2), we rely upon the available off-glacier data and lapse rates that  
671 are not derived in a consistent manner. The derivation of flowline distances from the DEM are  
672 also not consistent between the prior studies (Shea and Moore, 2010; Carturan et al., 2015; Shaw  
673 et al., 2017; Bravo et al., 2019a; Troxler et al., 2020), and may hold some small influence on the  
674 derived parameterisations (Table 3), particularly at lateral locations on the glacier (not explored  
675 here), that can be subject to different micro-meteorological effects (van de Wal, 1992; Hannah et  
676 al., 2000; Shaw et al., 2017). Equally, the uncertainty of the actual observations (e.g. section 3.2)  
677 is hard to clearly define due the variable instrumentation (sensors and radiation shielding), on-  
678 glacier location and local topographic and micro-meteorological effects of each study site (Table  
679 2). Because our study, and many similar studies of this kind, did not have artificially ventilated  
680 radiation shields available, the uncertainty of the measured  $T_a$  is difficult to quantify. We consider  
681 this to be less problematic at large flowline distances, where good ventilation to the sensors is  
682 often provided by the glacier katabatic wind layer even under warm conditions. However, at short  
683 flowline distances in the glacier accumulation zones, uncertainty of both the on-glacier  
684 observations and ambient  $T_a$  extrapolation is larger. Artificially ventilated radiation shields are  
685 not commonplace in glaciological research due to the additional power demands that often cannot  
686 be met, though would be strongly encouraged for further research into the temperature sensitivity  
687 of mountain glaciers. Further work on a unified model of estimating  $T_a$  should need to address  
688 these issues, perhaps with further, dedicated analyses.

689  
690 In our study, we apply the parameterisation of Carturan et al. (2015) to derive along-flowline  
691 values of the theoretical onset of the *KBL* ( $T^*$ ). While these values appear appropriate for our case  
692 studies (based upon manual inspection), they were derived for a smaller sample size of total  
693 observations. We experimented with a static  $T^*$  value of 5°C in order to test the sensitivity of our  
694 analysis to the assumptions of  $T^*$ , though we found negligible sensitivity of derived  $k2$  on  $T^*$  (not  
695 shown). Similarly, a sensitivity to the choice of constant lapse rate for those sites without available  
696 lapse rate information (Table 2) proved to have only a small influence on the derived  $k1$  and  $k2$   
697 values.

698  
699 Finally, in this study we assess temperature sensitivity based upon ambient air temperatures above  
700 the  $T^*$  threshold. This is partly different to the ‘climatic sensitivity’ presented by earlier works  
701 (Greuell et al., 1997; Greuell and Böhm, 1998; Oerlemans, 2001; 2010), which considered an ‘all-  
702 hour’ temperature sensitivity value (i.e. not thresholding sensitivities by katabatic wind onset -  
703 Figure 1b). However, ignoring the differences in temperature sensitivity before and after the onset  
704 of the *KBL* (Figure 1c, Figure 5) is arguably an over-simplification and does not enable one to  
705 correctly describe the observed behaviours (Shea and Moore, 2010; Jiskoot and Mueller, 2012).  
706 Accordingly, we caution somewhat the direct comparison of the temperature sensitivity presented  
707 here and the ‘climatic sensitivity’ of previous works.

708 We consider the SM10 approach and the use of  $k2$  to be an appropriate indicator of temperature  
709 sensitivity for mountain glaciers in future work of this type. This approach is an easily adaptable  
710 method for calculating glacier temperature sensitivity and thus estimating on-glacier  $T_a$ . However,  
711 the competing effects of glacier katabatic and up-valley winds/debris or valley warming need to  
712 be incorporated to address the challenges that less simplistic methods (i.e. ModGB) were designed  
713 for.

714  
715 Based upon the findings of this work, we recommend that future research i) attempt to standardise,  
716 where possible, the measurement and comparison of off- and on-glacier air temperature, exploring  
717 the use of artificially-ventilated radiation shields that are less prone to heating errors (Georges

718 and Kaser, 2002; Carturan et al., 2015), ii) instrument glaciers of varying size in the same  
719 catchment to explore the relative importance of glacier size and local meteorological conditions  
720 (Figure 7), and iii) model the detailed interactions of air flows on glacier termini using, for  
721 example, large eddy simulations (Sauter and Galos, 2016; Bonekamp et al., 2020) in order to  
722 identify possible drivers of the observed increase in temperature sensitivity for certain glacier  
723 areas (point ‘4’ in Figure 1).

724

## 725 **7. Conclusions**

726 We presented a new dataset of distributed on-glacier air temperatures for three glaciers of  
727 different size in the south-east Tibetan Plateau during two summers (July - September). We  
728 analysed the along-flowline air temperature distribution for all three glaciers and compared them  
729 to the estimated ambient temperatures derived from several, local off-glacier stations. Using this  
730 information, we parameterised the along-flowline temperature sensitivities of these glaciers using  
731 the method proposed by Shea and Moore (2010) and presented the results in the context of several  
732 available distributed on-glacier datasets. The key findings of this work are:

733

- 734 1. For our Tibetan case study, on-glacier air temperatures at short flowline distances display  
735 a high temperature sensitivity (i.e. demonstrate a relationship with off-glacier air  
736 temperature that is close to 1). We therefore confirm earlier evidence regarding the high  
737 temperature sensitivity of high elevation, small glaciers (flowline distances < 1000 m) to  
738 external climate, and thus future warming.
- 739 2. The largest differences between observed on-glacier and estimated off-glacier air  
740 temperatures are found for the warmest off-glacier hours, during drier, clear sky  
741 conditions of the summer monsoon period.
- 742 3. Above the established onset of the katabatic boundary layer, temperature sensitivity to  
743 ambient temperature decreases rapidly up to ~2000-3000 m along the glacier flowline.  
744 Beyond this distance, both the Tibetan glaciers and other datasets of the literature show  
745 a slower decrease of temperature sensitivity.
- 746 4. A parameterisation for the temperature sensitivity of the Tibetan study glaciers implies a  
747 similar boundary layer effect compared to the existing parameterisation of Shea and  
748 Moore (2010). The climatology of a given region may influence the magnitude of the  
749 glacier's temperature sensitivity, though no clear relationships with the climatology of the  
750 glacier sites are found, thus suggesting the stronger role of local meteorological or  
751 topographic effects on the along-flowline pattern of  $T_a$  variability.
- 752 5. The terminus of some glaciers is associated with other warm air processes, possibly due  
753 to boundary layer divergence, warm up-valley winds, large glacier slope changes or  
754 debris cover/valley heating. We find that these effects are evident only beyond ~70% of  
755 the total glacier flowline distance, although further work is required to explain this  
756 behaviour. A better understanding of temperature variability for this lower 30% is highly  
757 important as this part of the glacier is most affected by ablation.

758

759 In summarising the findings from all available distributed on-glacier datasets to date, we identify  
760 some key directions for future work on this subject. This includes comparing local influences of  
761 glacier size and micro-meteorology and standardising measurement practices, where possible, to  
762 enable the construction of a generalised model for on-glacier air temperature estimation.

763

## 764 **Acknowledgements**

765 Funding for the instrumentation of the Parlung catchment was provided by NSFC project  
766 (91647205 and 41961134035) and Newton Advanced Fellowship (NA170325). This project has  
767 received funding from the European Research Council (ERC) under the European Union's  
768 Horizon 2020 research and innovation programme grant agreement No 772751, RAVEN, "Rapid  
769 mass losses of debris covered glaciers in High Mountain Asia". Á. Ayala acknowledges support

770 from a FONDECYT project (number 3190732) and C. Bravo from the ANID Becas Chile PhD  
771 scholarship program. The authors kindly acknowledge the sharing of global datasets or  
772 parameters provided to aid this analysis, explicitly M. Nolan (McCall Glacier), P. Smeets and  
773 IMAU, Utrecht (Pasterze Glacier), DGA, Chile (Universidad Glacier and Greve Glacier) and L.  
774 Carturan (AVDM, Italy). The Peyto Glacier data used this paper were provided by the Global  
775 Water Futures (GWF) Programme and by J. Pomeroy and D. Pradhananga. E. Ludewig is thanked  
776 for the provision of off-glacier temperature records at Sonnblick station, Austria. Additionally we  
777 recognise the hard work involved in obtaining and sharing all of the datasets acquired and the  
778 acknowledgements of those works. Scientific editor T. Sauter, L. Carturan and one anonymous  
779 reviewer are thanked for their insightful and constructive comments that have improved the  
780 quality of the manuscript.

#### 781 **Author contributions**

782 TES and WY discussed and designed the research plan with Parlung data provided by WY and  
783 CZ. Additional data and analysis was provided by AA and CB. TES wrote the manuscript with  
784 scientific input from all co-authors.

#### 785 **Data availability**

786 Calculated flowlines and temperature sensitivities are available at the following Zenodo  
787 repository: <http://doi.org/10.5281/zenodo.3937777>

#### 788 **Competing Interests**

789 The authors declare that they have no conflicting interests.

790

#### 791 **References**

792 ASF DAAC: ALOS PALSAR\_Radiometric\_Terrain\_Corrected\_low\_res; Includes Material ©  
793 JAXA/METI 2007. Accessed through ASF DAAC 20<sup>th</sup> March, 2020.  
794 DOI: 10.5067/JBYK3J6HFSVF, 2020

795 Arnold, N. S., Rees, W. G., Hodson, A. J., & Kohler, J.: Topographic controls on the surface  
796 energy balance of a high Arctic valley glacier. *J. Geophys. Res.*, 111(F2), F02011.  
797 <https://doi.org/10.1029/2005JF000426>, 2006

798 Ayala, A., Pellicciotti, F., & Shea, J.: Modeling 2m air temperatures over mountain glaciers:  
799 Exploring the influence of katabatic cooling and external warming. *J. Geophys. Res: Atmos*, 120,  
800 1–19. <https://doi.org/10.1002/2015JD023137> , 2015

801 Betts, A. K., Chan, D. Z., & Desjardins, R. L.: Near-Surface Biases in ERA5 Over the Canadian  
802 Prairies. *Front. Environ. Sci.*, 7. <https://doi.org/10.3389/fenvs.2019.00129> , 2019

803 Bonekamp, P. N. J., Heerwaarden, C. C. Van, Steiner, J. F., & Immerzeel, W. W.: Using 3D  
804 turbulence-resolving simulations to understand the impact of surface properties on the energy  
805 balance of a debris-covered glacier. *Cryosph.*, 14, 1611–1632. [https://doi.org/10.5194/tc-14-1611-](https://doi.org/10.5194/tc-14-1611-2020)  
806 [2020](https://doi.org/10.5194/tc-14-1611-2020) , 2020

807 Bravo, C., Quincey, D. J., Ross, A. N., Rivera, A., Brock, B. W., Miles, E., & Silva, A.: Air  
808 Temperature Characteristics , Distribution , and Impact on Modeled Ablation for the South  
809 Patagonia Ice field. *J. Geophys. Res: Atmos*, 124, 907–925.  
810 <https://doi.org/10.1029/2018JD028857> , 2019a

- 811 Bravo, C., Bozkurt, D., Gonzalez-reyes, Á., Quincey, D. J., Ross, A. N., Farias-Barahona, D., &  
812 Rojas, M.: Assessing Snow Accumulation Patterns and Changes on the Patagonian Icefields.  
813 *Frontiers in Environmental Science*, 7(March), 1–18. <https://doi.org/10.3389/fenvs.2019.00030> ,  
814 2019b
- 815 Bravo, C., Lorlaux, T., Rivera, A., & Brock, B. W.: Assessing glacier melt contribution to  
816 streamflow at Universidad Glacier, central Andes of Chile. *Hydrol. Earth Syst. Sci*, 21, 3249–  
817 3266. <https://doi.org/10.5194/hess-21-3249-2017> , 2017
- 818 Brock, B. W., Mihalcea, C., Kirkbride, M. P., Diolaiuti, G., Cutler, M. E. J., & Smiraglia, C.:  
819 Meteorology and surface energy fluxes in the 2005–2007 ablation seasons at the Miage debris-  
820 covered glacier, Mont Blanc Massif, Italian Alps. *J. Geophys. Res.*, 115, D09106.  
821 <https://doi.org/10.1029/2009JD013224> , 2010
- 822 Caidong, C., & Sorteberg, A.: Modelled mass balance of Xibu glacier, Tibetan Plateau: Sensitivity  
823 to climate change. *J. Glaciol.*, 56(196), 235–248. <https://doi.org/10.3189/002214310791968467> ,  
824 2010
- 825 Carturan, L., Cazorzi, F., De Blasi, F., & Dalla Fontana, G.: Air temperature variability over three  
826 glaciers in the Ortles–Cevedale (Italian Alps): effects of glacier fragmentation, comparison of  
827 calculation methods, and impacts on mass balance modeling. *Cryosph.*, 9(3), 1129–1146.  
828 <https://doi.org/10.5194/tc-9-1129-2015> , 2015
- 829 Copernicus Climate Change Service (C3S): ERA5: Fifth generation of ECMWF atmospheric  
830 reanalyses of the global climate . Copernicus Climate Change Service Climate Data Store (CDS),  
831 Available at: <https://cds.climate.copernicus.eu/cdsapp#!/home>. Accessed 05/05/2020 , 2017
- 832 Ding, B., Yang, K., Yang, W., He, X., Chen, Y., Lazhu, ... Yao, T.: Development of a Water and  
833 Enthalpy Budget-based Glacier mass balance Model (WEB-GM) and its preliminary validation.  
834 *Water Resour. Res.*, 53(4), 3146–3178. <https://doi.org/10.1002/2016WR018865> , 2017
- 835 Gabbi, J., Carenzo, M., Pellicciotti, F., Bauder, A., & Funk, M.: A comparison of empirical and  
836 physically based glacier surface melt models for long-term simulations of glacier response. *J.*  
837 *Glaciol.*, 60(224), 1140–1154. <https://doi.org/10.3189/2014JoG14J011> , 2014
- 838 Gardner, A. S., Sharp, M. J., Koerner, R. M., Labine, C., Boon, S., Marshall, S. J., ... Lewis, D.:  
839 Near-Surface Temperature Lapse Rates over Arctic Glaciers and Their Implications for  
840 Temperature Downscaling. *J. Clim.*, 22(16), 4281–4298.  
841 <https://doi.org/10.1175/2009JCLI2845.1>, 2009
- 842 Georges, C., & Kaser, G.: Ventilated and unventilated air temperature measurements for glacier-  
843 climate studies on a tropical high mountain site. *J. Geophys. Res.*, 107(D24), 4775.  
844 <https://doi.org/10.1029/2002JD002503> , 2002
- 845 Greuell, W., & Böhm, R.: 2 m temperatures along melting mid-latitude glaciers , and implications  
846 for the sensitivity of the mass balance to variations in temperature. *J. Glaciol.*, 44(146), 9–20. ,  
847 1998
- 848 Greuell, W., Knap, W. H., & Smeets, P. C.: Elevational changes in meteorological variables along  
849 a midlatitude glacier during summer. *J. Geophys. Res.*, 102(D22), 25941.  
850 <https://doi.org/10.1029/97JD02083> , 1997



- 851 Hannah, D. M., Gurnell, A. M., & McGregor, G. R.: Spatio-temporal variation in microclimate,  
852 the surface energy balance and ablation over a cirque glacier. *Int. J. Climatol.*, 20(7), 733–758.  
853 [https://doi.org/10.1002/1097-0088\(20000615\)20:7](https://doi.org/10.1002/1097-0088(20000615)20:7) , 2000
- 854 Heynen, M., Miles, E., Ragetti, S., Buri, P., Immerzeel, W., & Pellicciotti, F.: Air temperature  
855 variability in a high elevation Himalayan catchment. *Ann. Glaciol.*, 57(71),  
856 <https://doi.org/10.3189/2016AoG71A076> , 2016
- 857 Huintjes, E., Sauter, T., Schröter, B., Maussion, F., Yang, W., Kropáček, J., ... Schneider, C.:  
858 Evaluation of a Coupled Snow and Energy Balance Model for Zhadang Glacier, Tibetan Plateau,  
859 Using Glaciological Measurements and Time-Lapse Photography. *Arctic, Antarct. Alp. Res.*,  
860 47(3), 573–590. <https://doi.org/10.1657/AAAR0014-073> , 2015
- 861 Immerzeel, W. W., Petersen, L., Ragetti, S., & Pellicciotti, F.: The importance of observed  
862 gradients of air temperature and precipitation for modeling runoff from a glacierized watershed.  
863 *Water Resour. Res.*, 50, 2212–2226. <https://doi.org/10.1002/2013WR014506> , 2014
- 864 Jiskoot, H., & Mueller, M. S.: Glacier fragmentation effects on surface energy balance and runoff:  
865 field measurements and distributed modelling. *Hydrol. Process.*, 26(12), 1861–1875.  
866 <https://doi.org/10.1002/hyp.9288> , 2012
- 867 Jobst, A. M., Kingston, D. G., Cullen, N. J., & Sirguey, P.: Combining thin-plate spline  
868 interpolation with a lapse rate model to produce daily air temperature estimates in a data-sparse  
869 alpine catchment. *Int. J. Climatol.*. <https://doi.org/10.1002/joc.4699> , 2016
- 870 Marshall, S. J., Sharp, M. J., Burgess, D. O., & Anslow, F. S.: Near-surface-temperature lapse  
871 rates on the Prince of Wales Icefield, Ellesmere Island, Canada: implications for regional  
872 downscaling of temperature. *Int. J. Climatol.*, 27, 1549–1555. <https://doi.org/10.1002/joc> , 2007
- 873 Maurer, J. M., Schaefer, J. M., Rupper, S., & Corley, A.: Acceleration of ice loss across the  
874 Himalayas over the past 40 years. *Sci. Adv.*, 5, 1–12., 2019
- 875 Minder, J. R., Mote, P. W., & Lundquist, J. D.: Surface temperature lapse rates over complex  
876 terrain: Lessons from the Cascade Mountains. *J. Geophys. Res.*, 115(D14), D14122.  
877 <https://doi.org/10.1029/2009JD013493> , 2010
- 878 Mölg, T., Maussion, F., Yang, W., & Scherer, D.: The footprint of Asian monsoon dynamics in  
879 the mass and energy balance of a Tibetan glacier. *Cryosph.*, 6(6), 1445–1461.  
880 <https://doi.org/10.5194/tc-6-1445-2012> , 2012
- 881 Munro, D. S.: Linking the weather to glacier hydrology and mass balance at Peyto glacier. *Peyto*  
882 *Glacier: One Century of Science*. National Hydrology Research Institute Science Report #8. ,  
883 2006
- 884 Munro, D. S., & Marosz-Wantuch, M.: Modeling Ablation on Place Glacier, British Columbia,  
885 from Glacier and Off-glacier Data Sets. *Arctic, Antarct. Alp. Res.*, 41(2), 246–256.  
886 <https://doi.org/10.1657/1938-4246-41.2.246> , 2009
- 887 Nolin, A. W., Phillippe, J., Jefferson, A., & Lewis, S. L.: Present-day and future contributions of  
888 glacier runoff to summertime flows in a Pacific Northwest watershed: Implications for water  
889 resources. *Water Resour. Res.*, 46(12). <https://doi.org/10.1029/2009WR008968> , 2010

- 890 Oerlemans, B. J., & Grisogono, B.: Glacier winds and parameterisation of the related surface heat  
891 fluxes. *Tellus*, 54, 440–452. , 2002
- 892 Oerlemans, J.: The microclimate of valley glaciers. Utrecht Publishing and Archiving Services,  
893 Universiteitsbibliotheek, Utrecht. , 2010
- 894 Oerlemans, J.: *Glaciers and Climate Change.* , 2001
- 895 Pellicciotti, F., Helbing, J., Rivera, A., Favier, V., Corripio, J. G., Araos, J., ... Carenzo, M.: A  
896 study of the energy balance and melt regime on Juncal Norte Glacier , semi-arid Andes of central  
897 Chile , using melt models of different complexity. *Hydrol. Process.*, 22, 3980–3997.  
898 <https://doi.org/10.1002/hyp> , 2008
- 899 Petersen, L., & Pellicciotti, F.: Spatial and temporal variability of air temperature on a melting  
900 glacier: Atmospheric controls, extrapolation methods and their effect on melt modeling, Juncal  
901 Norte Glacier, Chile. *J. Geophys. Res.*, 116(D23), D23109.  
902 <https://doi.org/10.1029/2011JD015842> , 2011
- 903 Petersen, L., Pellicciotti, F., Juszak, I., Carenzo, M., & Brock, B. W.: Suitability of a constant air  
904 temperature lapse rate over an Alpine glacier: testing the Greuell and Böhm model as an  
905 alternative. *Ann. Glaciol.*, 54(63), 120–130. <https://doi.org/10.3189/2013AoG63A477> , 2013
- 906 Pradhananga, D., Pomeroy, J. W., Aubry-Wake, C., Munro, D. S., Shea, J., Demuth, M. N., Kirat,  
907 N. H., Menounos, B., and Mukherjee, K.: Hydrometeorological, glaciological and geospatial  
908 research data from the Peyto Glacier Research Basin in the Canadian Rockies, *Earth Syst. Sci.*  
909 *Data Discuss.*, <https://doi.org/10.5194/essd-2020-219>, in review, 2020.
- 910 Ragetti, S., Immerzeel, W. W., & Pellicciotti, F.: Contrasting climate change impact on river  
911 flows from high-altitude catchments in the Himalayan and Andes Mountains. *Proc. Natl. Acad.*  
912 *Sci.*, 113(33). <https://doi.org/10.1073/pnas.1606526113> , 2016
- 913 Rets, E. P., Popovnin, V. V, Toropov, P. A., Smirnov, A. M., Tokarev, I. V, Chizhova, J. N., ...  
914 Kireeva, M. B.: Djankuat glacier station in the North Caucasus , Russia : a database of  
915 glaciological , hydrological , and meteorological observations and stable isotope sampling results  
916 during 2007 – 2017. *Earth Syst. Sci. Data*, 1463–1481.  
917 <https://doi.org/https://doi.org/10.5194/essd-11-1463-2019> , 2019
- 918 Sauter, T., & Galos, S. P.: Effects of local advection on the spatial sensible heat flux variation on  
919 a mountain glacier. *Cryosph.*, 10, 2887–2905. <https://doi.org/10.5194/tc-10-2887-2016> , 2016
- 920 Schwanghart, W., Kuhn, N, J.: TopoToolbox: A set of Matlab functions for topographic analysis,  
921 *Environmental Modelling & Software*, 25 (6), 770-781.  
922 <https://doi.org/10.1016/j.envsoft.2009.12.002> . , 2010
- 923 Shaw, T. E., Brock, B. W., Ayala, A., Rutter, N., & Pellicciotti, F.: Centreline and cross-glacier  
924 air temperature variability on an Alpine glacier: assessing temperature distribution methods and  
925 their influence on melt model calculations. *J. Glaciol.*, 1–16. <https://doi.org/10.1017/jog.2017.65>  
926 , 2017
- 927 Shaw, T., Brock, B., Fyffe, C., Pellicciotti, F., Rutter, N., & Diotri, F.: Air temperature  
928 distribution and energy balance modelling of a debris-covered glacier. *J. Glaciol.*, 62(231), 185–  
929 198. <https://doi.org/10.1017/jog.2016.31> , 2016

- 930 Shea, J. M., & Moore, R. D.: Prediction of spatially distributed regional-scale fields of air  
931 temperature and vapor pressure over mountain glaciers. *J. Geophys. Res.*, 115(D23), D23107.  
932 <https://doi.org/10.1029/2010JD014351> , 2010
- 933 Steiner, J. F. and Pellicciotti, F.: Variability of air temperature over a debris-covered glacier in  
934 the Nepalese Himalaya, *Ann. Glaciol.*, 57(71), 295–307, doi:10.3189/2016AoG71A066, 2016.
- 935 Strasser, U., Corripio, J. G., Pellicciotti, F., Burlando, P., Brock, B. W., & Funk, M.: Spatial and  
936 temporal variability of meteorological variables at Haut Glacier d’Arolla (Switzerland) during the  
937 ablation season 2001: Measurements and simulations. *J. Geophys. Res.*, 109, D03103.  
938 <https://doi.org/10.1029/2003JD003973> , 2004
- 939 Troxler, P., Ayala, Á., Shaw, T. E., Nolan, M., Brock, B. W., & Pellicciotti, F.: Modelling spatial  
940 patterns of near-surface air temperature over a decade of melt seasons on McCall Glacier, Alaska.  
941 *J. Glaciol.*, 1–15. <https://doi.org/https://doi.org/10.1017/jog.2020.12> , 2020
- 942 van de Wal, R. S. W., Oerlemans, J., & Van Der Hage, J. C.: A study of ablation variations on  
943 the tongue of Hintereisferner, Austrian Alps. *J. Glaciol.*, 38(130), 319–324. , 1992
- 944 van den Broeke, M. R.: Momentum , Heat , and Moisture Budgets of the Katabatic Wind Layer  
945 over a Midlatitude Glacier in Summer. *J. Appl. Meteorol.*, 36(1987), 763–774. , 1997
- 946 Wang, R., Liu, S., Shangguan, D., Radić, V., & Y, Z.: Spatial Heterogeneity in Glacier Mass-  
947 Balance. *Water*, 11(776), 1–21. <https://doi.org/doi:10.3390/w11040776> , 2019
- 948 Yang, W., Guo, X., Yao, T., Yang, K., Zhao, L., Li, S., & Zhu, M.: Summertime surface energy  
949 budget and ablation modeling in the ablation zone of a maritime Tibetan glacier. *J. Geophys. Res.*  
950 *Atmos.*, 116(14), 1–11. <https://doi.org/10.1029/2010JD015183> , 2011
- 951 Yang, W., Yao, T., Guo, X., Zhu, M., Li, S., & Kattel, D. B.: Mass balance of a maritime glacier  
952 on the southeast Tibetan Plateau and its temperature sensitivity. *J. Geophys. Res. Atmos.*, 118(17),  
953 9579–9594. <https://doi.org/10.1002/jgrd.50760> , 2013
- 954 Zhao, L., Tian, L., Zwinger, T., Ding, R., Zong, J., Ye, Q., & Moore, J. C.: Numerical simulations  
955 of Gurenhekou glacier on the Tibetan Plateau. *J. Glaciol.*, 60(219), 71–82.  
956 <https://doi.org/10.3189/2014JoG13J126> , 2014
- 957 Zhu, M., Yao, T., Yang, W., Maussion, F., Huintjes, E., & Li, S.: Energy- and mass-balance  
958 comparison between Zhadang and Parlung No. 4 glaciers on the Tibetan Plateau. *J. Glaciol.*,  
959 61(227), 595–607. <https://doi.org/10.3189/2015JoG14J206> , 201  
960